T.R.
GEBZE TECHNICAL UNIVERSITY
GRADUATE SCHOOL OF NATURAL AND APPLIED SCIENCES

PREPARATION AND CHARACTERIZATION OF NANOMAGNETS SHOWING SPIN-TRANSFER TORQUE EFFECTS

ŞABAN TIRPANCI
A THESIS SUBMITTED FOR THE DEGREE OF
DOCTOR OF PHILOSOPHY
DEPARTMENT OF PHYSICS

GEBZE
2015

T.R.

GEBZE TECHNICAL UNIVERSITY

GRADUATE SCHOOL OF NATURAL AND APPLIED SCIENCES

PREPARATION AND CHARACTERIZATION OF NANOMAGNETS SHOWING SPIN-TRANSFER TORQUE EFFECTS

ŞABAN TIRPANCI

A THESIS SUBMITTED FOR THE DEGREE OF DOCTOR OF PHILOSOPHY

DEPARTMENT OF PHYSICS

THESIS SUPERVISOR

PROF. DR. BEKİR AKTAŞ

GEBZE

2015

T.C.
GEBZE TEKNİK ÜNİVERSİTESİ
FEN BİLİMLERİ ENSTİTÜSÜ

SPİN TRANSFER TORK ETKİSİ SERGİLEYEN NANOMAGNETLERİN HAZIRLANMASI VE KARAKTERİZASYONLARININ BELİRLENMESİ

ŞABAN TIRPANCI
DOKTORA TEZİ
FİZİK ANABİLİM DALI

DANIŞMANI
PROF. DR. BEKİR AKTAŞ

GEBZE
2015

DOKTORA JÜRİ ONAY FORMU

GTÜ Fen Bilimleri Enstitüsü Yönetim Kurulu'nun 24/06/2015 tarih ve 2015/39 sayılı kararıyla oluşturulan jüri tarafından 03/07/2015 tarihinde tez savunma sınavı yapılan Şaban TIRPANCI'ın tez çalışması Fizik Anabilim Dalında DOKTORA tezi olarak kabul edilmiştir.

JÜRİ

ÜYE (TEZ DANIŞMANI)	:	Prof Dr. Bekir AKTAŞ
ÜYE	:	Prof. Dr. Bulat RAMİ
ÜYE	:	Doç. Dr. Hüseyin KAVAS
ÜYE	:	Doç. Dr. Savaş BERBER
ÜYE	:	Prof. Dr. Ramis Mustafa ÖKSÜZOĞLU

ONAY

Gebze Teknik Üniversitesi Fen Bilimleri Enstitüsü Yönetim Kurulu'nun

......./......./....... tarih ve ..../....... sayılı kararı.

İMZA/MÜHÜR

SUMMARY

In last two decades, magnetization dynamics induced by spin-transfer torque (STT) have attracted much attention due to possible spintronic applications. To study STT effect, there are several geometries. One of the most preferable geometries that shows STT is lithographically defined nanopillar array. Electron beam (e-beam) writer and scanning electron microscope (SEM) are employed to write and image these nanopillars. Charging effect is serious issue during the employment of e-beam writer and SEM on insulating substrates like MgO.

On the other hand, Heusler Alloys form a large family with over 1500 members. Although Heusler Alloys are known for a long time, new properties and functions of them were discovered in recent years. Because of physical and structural properties (high spin polarization, high Curie temperature, etc.) Co_2MnSi is one of the promising candidates for future spintronic applications.

In this work, charging problem was solved without using conductive polymers or depositing conductive element in each step of the fabrication processes. After employment of state of art nanofabrication techniques (litography), ellipsoidal nanopillars with a cross-section of 75x120 nm^2 were patterned from raw Cr/Ag/Co2MnSi/Ag/Co2MnSi/Ag/Au mutilayer stack. Magnetotransport measurements of an individual nanopillar structure exhibit 2% GMR. Current induced magnetizaton reversal measurements on each individual nanopillar show existence of STT, and also confirm the success of modification in nanofabrication process.

Key Words: Giant Magnetoresistance, Spin-transfer torque, Heusler alloys, half metallic alloys, charging effect, nanolithography, nanopillar fabrication.

ÖZET

Son yirmi yılda, olası Spintronik uygulamaları nedeniyle, spin transfer tork (STT) tarafından uyarılan mıknatıslanma dinamikleri büyük ilgi çekmektedir. STT etkisini incelemek için çeşitli geometriler mevcuttur. STT sergileyen bu geometrilerden en çok tercih edilenlerden biri litografik olarak tanımlanan nanosütunlardır. Elektron ışın demeti yazıcı ve taramalı elektron mikroskobu (SEM) bu nanosütunların yazma ve görüntülenmesi için kullanılmaktadır. Film desenleme sırasında oluşan yük birikimi, MgO gibi yalıtkan alttaşlarda, e-ışın demeti yazıcı ve SEM işlemlerinde çok ciddi problem oluşturmaktadır.

Bilindiği gibi, Heusler Alaşımları, 1500 üyesi ile olan dev bir ailedir. Heusler Alaşımları uzun süredir bilinmesine rağmen, son yıllarda bunların yeni özellikleri ve fonksiyonları keşfedilmiştir. Fiziksel ve yapısal özellikleri (yüksek spin polarizasyon, yüksek Curie sıcaklığı, vb.) Co_2MnSi alaşımını gelecekteki spintronik uygulamaları için umut verici adaylardan biri kılmaktadır.

Bu çalışmada, yük birikimi sorunu, her aşamada iletken element veya iletken polimerler biriktirilmesi yöntemi kullanmadan çözüldü. Çok katmanlı Cr/Ag/Co2MnSi/Ag/Co2MnSi/Ag/Au filmleri üst düzey nanofabrikasyon teknikleri ile işlenerek, 75x120 nm^2 yüzey kesitine sahip elipsoit nano-sütunlar üretildi. Üretilen bir nanosütun üzerinde yapılan manyetotransport ölçümleri ile % 2 civarında manyeto direnç gözlenmiştir. Her bir nanosütun üzerinde yapılan manyetizasyon ters çevrimi ölçümleri (magnetization reversal) STT etkisinin indüklenebildiğini ve aynı zamanda nanofabrikasyon sürecinde gerekli önemli geliştirmeler başarıldığını kanıtlamıştır.

Anahtar Kelimeler: Devasa Manyetodirenç, Spin-Transfer Tork, Heusler Alaşımları,Yarı Manyetik Alaşımlar, Yük Birikimi, Nanolitografi, Nanosütun Fabrikasyonu.

ACKNOWLEDGEMENTS

In my opinion most difficult part of writing thesis is acknowledgements part. Because, many friends and colleages supported and encouraged me during this work. At the beginning I want to apologize to those that I forgot to mention name by name.

First of all, I would like to express my deep and sincere gratitude to my supervisors, Prof. Bekir Aktaş and PD Dr. Daniel Bürgler. Prof. Aktaş; his support, helps and encouragement gave me great motivation. Thanks for your patience and continuous support. You were more than Phd supervisor, you always treat as a friend. I learned a lot from you.

I wish to express my sincere thanks to Prof Bulat Rami and Prof Claus M. Schneider who accepted me as a guest researcher in his group. Without their support it was impossible to write these pages.

Many thanks to Dr. Şaşıoğlu. From my first day to submission, I received many support from him and his family in Julich.

My friends in PGI-6, Hatice, Raje, Zhong, Christian; you will be never forgotten. Thank you Volker. All I know about lithography, I learned from you. Clean room people, Ms. Bunte, Dr. Mörs, Dr. Lehmann, Dr. Trellenkamp, Mr. Bochem and the others, thank you all.

My friends in GTU, when i need help you were always ready to help me. Thanks for everything.

Most importantly, I would like to thank to each member of my family. Thank you for everything. My father has passed away (04.02.15) during writing this thesis. I owe and miss him so much. And my wife Merve, thanks for your love, patience and support.

Finally I would like thank to TUBITAK and HELMHOLTZ associations who gave finantial support under the collaborative agreement (Project No: IK-TR-06)

TABLE of CONTENTS

	Page
SUMMARY	v
ÖZET	vi
ACKNOWLEDMENTS	vii
TABLE of CONTENTS	viii
LIST of ABBREVIATIONS and ACRONYMS	x
LIST of FIGURES	xii
1. INTRODUCTION	1
2. THEORY	5
2.1. Spin dependent transport	5
2.1.1. Anisotropic magnetoresistance effect (AMR)	6
2.1.2. Giant magnetoresistance (GMR)	7
2.1.2.1. What is GMR?	7
2.1.2.2. Physical picture of GMR effect	10
2.1.3. Tunnel magnetoresistance effect (TMR)	13
2.1.4. Spin-transfer torque (STT)	14
2.1.4.1. Historical background and prior works	14
2.1.4.2. Theoretical background	17
2.1.4.3. Geometries for STT	22
2.1.4.4. Current induced magnetization dynamics	24
2.1.5. Spin transfer oscillator	28
2.1.6. STT magnetic random access memory (STT MRAM)	28
2.2. Heusler alloys	30
3. EXPERİMENTAL WORKS AND RESULTS	34
3.1. Nanofabrication and lithography	35

3.1.1. Deposition of Co2MnSi 35

3.1.2. Defining bottom electrodes and dissipater layer 35

3.1.3. Defining nanopillars by EBL 37

3.1.4. Insulation and opening contact windows 40

3.1.5. Deposition of top electrodes and removing connections 43

3.2. Experimental setup 45

3.3. GMR and current-induced magnetization switching 48

3.3.1. GMR results 49

3.3.2. Current-induced magnetization switching results 51

4. DISCUSSION AND CONCLUSION 53

REFERENCES 56

BIOGRAPHY 62

LIST of ABBREVIATIONS and ACRONYMS

Abbreviations and Acronyms		Explanations
$\vec{\mu}$	:	Magnet moment
ψ_{in}	:	Wave function of incoming Electron
ψ_{in}	:	Wave function of incoming Electron
$\vec{m}_{fixed}$	:	Magnetization vector of fixed layer
$\vec{m}_{free}$	:	Magnetization vector of free layer
μ_B	:	Bohr Magneton
$\vec{M}$	:	Magnetization Vector
M_s	:	Saturation magnetization
ψ_{ref}	:	Wave function of reflected Electron
ψ_{trans}	:	Wave function of transmitted Electron
A	:	Amper
Ag	:	Silver
Au	:	Gold
Co		Cobalt
ħ	:	Planck Constant
m	:	Mass of electron
Mn	:	Manganese
$\boldsymbol{S}$	:	Spin Angular Momentum
Si	:	Silicon
σ	:	Pauli Spin Matrix
$\boldsymbol{H}$	:	Effective magnetic field
Ω	:	Normalization Volume
α	:	Gilbert damping constant
γ	:	Gyromagnetic ratio
$\boldsymbol{\Phi}$	:	Current Spin Density Vector
$\boldsymbol{\nabla}$	:	Gradient operator

$\boldsymbol{\tau}$	:	Torque Vector
A	:	Cross section area
AMR	:	Anisotropic Magnetoresistance
AP	:	Antiparallel
CIP	:	Current in Plane
CPP	:	Current Perpendicular to Plane
DOS	:	Density of States
FM	:	Ferromagnetic
GMR	:	Giant magnetoresistance
MOKE	:	Magneto-optical Kerr effect
MR	:	Magnetoresistance
MRAM	:	Magnetic Random Access Memory
MTJ	:	Magnetic Tunnel Junction
NM	:	Non-magnetic
P	:	Parallel
R	:	Resistance
STO	:	Spin Transfer Oscillator
STT	:	Spin Transfer Torque
SV	:	Spin Valve
TMR	:	Tunnel magnetoresistance

LIST of FIGURES

Figure No:		Page
2.1:	First observations of the giant magnetoresistance effect.	8
2.2:	Geometries for GMR measurements.	9
2.3:	Illustration of GMR effect in CPP geometry.	10
2.4:	Two current model and corresponding to resistor model.	11
2.5:	Magnetic excitations in a Co/Cu multilayer due to a current injected through a point contact.	15
2.6:	Magnetic excitations and current-induced magnetization switching observed by the Cornell group.	16
2.7:	Current-induced magnetization switching in Co/Cu/Co nanopillars.	17
2.8:	Physical picture of the STT effect for the two directions (long horizontal arrows) of electron flux	19
2.9:	Current-induced magnetization reversal.	19
2.10:	Comparison of GMR vs. STT.	20
2.11:	Nanofabricated geometries for STT experiments.	23
2.12:	Torques in current-induced magnetization dynamics. Spin transfer torque’s direction depends on the direction of the current, either parallel or antiparallel to the damping torque. The latter case is shown in the figure.	27
2.13:	Current-induced magnetization.	27
2.14:	Cross-point architecture for an MRAM array	29
2.15:	Prototype of a MRAM and STT-MRAM.	30
2.16:	Comparison of the density of states of a metal, a semiconductor, and a half metal.	32
2.17:	$L2_1$ structure of the Co_2MnSi Heusler alloy.	32
2.18:	Density of states for Co_2MnSi. The spin-split band structure,	

insulating behavior for spin-down electrons of Co2MnSi. 33

3.1: Schematic view of the nanopillar structure for current-induced magnetization dynamics experiments. The current flows between the bottom and top electrodes and thus through the two ferromagnetic layers in the nanopillar. 36

3.2: Defining nanopillars by EBL. 39

3.3: Defining nanopillar structures 41

3.4: Insulation and opening contact windows 42

3.5: SEM view of an overetched contact window. The etching rate of capping layer of the nanopillar is higher than that of the insulators forming the contact window. For this reason the nanopillar is etched faster than the surrounding. 43

3.6: Deposition of top electrodes and removing dissipater connections. 44

3.7: Measurements system. 46

3.8: Preparation of the sample for measurements. 47

3.9: Sample holder with special chip carrier. 48

3.10: Giant magnetoresistance measurement at room temperature of nanopillar with cross section of 75x120 nm^2 .Applied current is 0.1 mA. The magnetic field is applied in the sample plane and parallel to the plane direction 50

3.11: Current-induced magnetization switching measurements 51

1. INTRODUCTION

Magnetic materials have attracted great attention in human life. They have a long history. As first example, loadstone (lead stone) was used more than two thousands years ago. First, it was used for fortune telling in ancient China. After centuries, it was started to be used as compasses to find direction and navigation in Chinese military. And today, magnetic materials are keeping the information that is stored in our computers. In addition to their usage in information storage industry, they are also widely used in sensor technology.

Until today many interesting properties of magnetism were discovered. Although magnetic materials are known for almost 2500 years, with progress in deposition technology and nanofabrication techniques, new properties of these materials were discovered in the last two decades. With these new properties they have an important place in information and sensor technologies. Today information technology depends on semiconductors and ferromagnetic materials. Stored bits in hard disk drives are read via ferromagnetic materials making direct use of their properties. Some of the sensors built into cars (e.g. position, angle and rotation sensors) are also based on properties of magnetic materials. There are lots of places where magnetic materials are used.

During the last two decades, researchers investigating magnetic materials exploit a new branch of physics and engineering called spintronics. What is spintronics? In traditional electronics, charges of electrons' are taken into account. But in spin electronics (spintronics), spin angular momenta of electrons' are also taken into account. In other words, the main idea and aim in spintronics is to control and manipulate the electron spin in addition to or even instead of its charge. Nowadays, spintronics is growing very rapidly.

Progress in nano and micro-fabrication techniques and deposition technology are the major reasons that bring about the progress in spintronics. By going to the nanoscale, researchers found the possibility to observe quantum properties of materials, which are dominant on the nanoscale. It is also important to emphasize the progress in deposition techniques. Nowadays it is possible produce a few

monolayer “thin” film stacks for science and industry. It also became possible to produce and investigate new ferromagnetic alloys (with high spin polarization), which have not been produced and investigated before.

The discovery of the Giant Magnetoresistance effect (GMR), in the late 1980s, by Peter Grünberg [1] and Albert Fert [2] is accepted to be the birthday of spintronics. This discovery took great attention. Not so long after the discovery of GMR effect in single crystal multilayers, Parkin [3] from IBM observed the GMR effect in polycrystalline multilayers. This significantly improved applicability in microelectronics industry. In the following, the GMR effect triggered a great revolution in chip industry, especially in data storage and magnetic sensors. Peter Grünberg and Albert Fert were honored for the discovery of GMR with the Nobel Prize in physics in 2007. GMR and other important magnetoresistance (MR) effects will be explained in the next chapter.

In 1996, a relatively short time after the discovery of GMR, the Spin Transfer Torque (STT) effect was predicted by Slonczewski [4] and Berger [5]. Basically, one understands STT as being reciprocal in the sense Newton’s third law to GMR. The spin transfer torque effect is a new mechanism that can control and manipulate the magnetism of a ferromagnet by current. Until the discovery of STT, an external magnetic field was used to control the magnetic orientation of a magnet. But STT is an alternative way that uses current instead of external magnetic field. Two years after the prediction the STT effect was experimentally proven by Tsoi [6], Sun [7], and Myers [8] in 1999. In 2000 the STT effect and spin transfer torque induced magnetic reversal were observed in nanopillar structures by Katine et al. [9]. Finally in 2003, current-driven steady state magnetic precession was achieved by the Cornell group [10]. This work has triggered the new area of the spin transfer torque effect, the so called spin transfer oscillators (STO). STT and STO will be discussed in the next chapter like MR effects.

Why is STT so important? The STT effect has two promising applications; this is why it attracted huge attention in a short period. The first one is the spin transfer torque magnetic random access memory (STT-MRAM) in information technology. In STT-MRAM, the bit of a cell value switches from 0 to 1 or from 1 to 0 by means of spin transfer torque with the current passing through the cell. Advantages of STT-

MRAM compared to other RAM technologies are small size, low power consumption, speed, and non-volatility. These aspects make STT-MRAM an ideal candidate for future memory technology.

The second application possibility for STT is spin transfer oscillators (STO). The STO is a strong candidate for future microwave generators, which are important for chip-to-chip wireless communication and radar communications. It has a wide spectrum and can be tuned by current and field. Its nanoscale size and compatibility with today's silicon chip production requirements take attentions on STO.

In this thesis, the GMR effect and current-induced magnetization switching by the STT effect was investigated. Co_2MnSi / Ag / Co_2MnSi nanopillar structures were prepared in the clean room environment with state of art nanofabrication techniques. A previously developed fabrication process [11] was modified for highly insulating substrates like MgO without using any conductive polymer photoresist or additional conductive element prior to each process step, where e-beam writing or e-beam imaging were used. The modified process prevents the charging effect without increasing the process time and cost.

In the second chapter a summary about the theory of GMR and some of other magnetoresistance effects (AMR: Anisotropic Magnetoresistance and TMR: Tunneling Magnetoresistance) as well as STT and STO will be given. In addition, there will be review and summary about previous works done in these fields. The second part of chapter 2 introduces Heusler alloys, especially Co_2MnSi, the Heusler alloy that is investigated in this work. I will give information about some physical and chemical properties of Co_2MnSi.

The third chapter describes the nanofabrication methods that I employed during construction of Co_2MnSi / Ag / Co_2MnSi nanopillars. Important aspects about reducing the charging effect on highly insulating substrate will be discussed. Modifications to the traditional Jülich nanopillar fabrication process to make it work for highly insulating substrates will be explained. The second part of the third chapter will give information about the measurement set-up that is used in this thesis.

The third part of third chapter will discuss the measurements taken in this work. After applying the modified Jülich nanopillar fabrication process to Co_2MnSi / Ag / Co_2MnSi multilayers, the resulting nanopillars were tested in magnetotransport measurements showing that the new process for nanofabrication is successful. GMR measurements and current-induced switching measurements will be presented in this chapter.

In Chapter four finally, a comparison between this work and the work done before will be given. I will also give a conclusion and an outlook.

2. THEORY

This chapter of the thesis is divided into two parts. The first part is devoted to spin-dependent transport. I will give brief information about magnetoresistance (MR) effects. Then, there will be information about the spin transfer phenomena and its applications. The second part is about Heusler alloys. Starting from the discovery of Heusler alloys, I will give information about the Co_2MnSi Heusler alloy, which is used for current-induced magnetization reversal experiments in this thesis.

2.1. Spin-dependent transport

As described in the introduction chapter, magnetic materials have a long history, but in the last two decades scientists have discovered breakthrough properties and effects of these materials. A short time period after these effects have been discovered, they have found applications in different areas science and technology. Because of the importance of this development, it is necessary to summarize these effects.

What is spintronics? An electron has charge and spin. In traditional electronics, the spin of the electron is not taken into account. The electron charge is used to manipulate and operate electronic devices. Simply, conventional electronic devices are based on just the electron charge. But electrons also have angular momentum which gives rise to the electron spin, a quantum property of electron. These angular momenta, spins, are the origin of magnetism. In the last two decades, scientists have investigated quantum properties of the electron. They have started experimental and theoretical studies on spin-dependent transport. With the progress of both theoretical and experimental works, a new branch of electronics has emerged, which is called “spintronics”. (spintronics is also called spinelectronics or magnetoelectronics). Shortly one can define spintronics as manipulating electrons via their spins.

Spintronics gained acceleration after the discovery of the Giant magnetoresistance (GMR) and Tunnel magnetoresistance (TMR) effects at room

temperature. With these discoveries, these magnetoresistance effects found application possibilities in industry, especially in data storage and sensor technology. In fact, read-heads in hard drives that we use in our computers base on the TMR effect.

On the other hand, the discovery of spin transfer torque (STT) canalized spintronics into brand new fields. The idea was to apply Newton's third law to GMR effect (it will be explained below). MRAM (Magnetic random access memory) using STT was prototyped and is presently being commercialized.

Up to now, just two magnetoresistance effects (GMR and TMR) are mentioned but there are more than two effects. For example: AMR (Anisotropic Magnetoresistance), Colossal magnetoresistance (CMR), Ballistic magnetoresistance (BMR) etc. But in this chapter only AMR, GMR, and TMR will be summarized.

2.1.1. Anisotropic magnetoresistance effect (AMR)

Anisotropic Magnetoresistance (AMR) is the dependence of resistivity on the angle between applied magnetic field and direction of the current. AMR was discovered in 1856 by Lord William Thomson Kelvin [11]. He was the first the use the term "magnetoresistance". Lord Kelvin measured the resistance of nickel and iron under different directions of applied magnetic field. He observed that the resistance varied according to the applied magnetic field. In other words, the measured resistances for the current parallel or perpendicular, respectively, to applied magnetic field were not the same. This effect is called Anisotropic Magnetoresistance (AMR).

The physical origin of AMR is spin-orbit coupling in ferromagnetic materials. The conduction (s) electrons are scattered by orbital angular momentum of 3d electrons. When the direction of the applied magnetic field is changed, the scattering ratio changes as well. Literally, when the magnetization and current direction becomes parallel, the scattering cross-section raises. When they are perpendicular, the scattering cross section decreases. Since the resistivity depends on scattering the resistance also changes. The change in the resistance is about 2%.

This effect has been used as magnetic sensor for a long time till the discovery of GMR. Even AMR sensors are still useful and are being used in sensor industry.

2.1.2. Giant magnetoresistance effect (GMR)

GMR effect was discovered by Peter Grünberg from Jülich and Albert Fert from Paris, separately and simultaneously, in 1988. This effect was first observed on the layered structures consisting of Fe and Cr, which were grown by Molecular Beam Epitaxy (MBE). Curves from the original publications are shown in Figure 2.1. The discovery of the GMR effect attracted great attention.

Compare to AMR, magnetoresistance values of GMR were significantly higher. This is why it is called as “Giant”. In 1990, Parkin [3] from IBM observed the GMR effect in polycrystalline structures. With this work, it became easier to use GMR for industrial applications and to replace AMR read-heads in Hard Disk Drives (HDD) with GMR read-heads.

By now the GMR effect has been used as magnetic field sensors, bio-sensors, read-heads in hard disk drives and many areas in science and industry. The discovery of GMR was a breakthrough in thin film magnetism and magnetotransport. As mentioned in the first chapter, discovery of the GMR is accepted as birth of spintronics and this discovery is the pioneer of many innovative works in science and technology. For all this importance and attraction, Peter Grünberg and Albert Fert have been awarded with Nobel Prize in Physics in 2007 for the discovery of GMR.

2.1.2.1. What is GMR?

To understand what GMR is, let’s consider a system that consists of two ferromagnetic (F) layers separated by a non magnetic (N) metal layer (Figure 2.2).

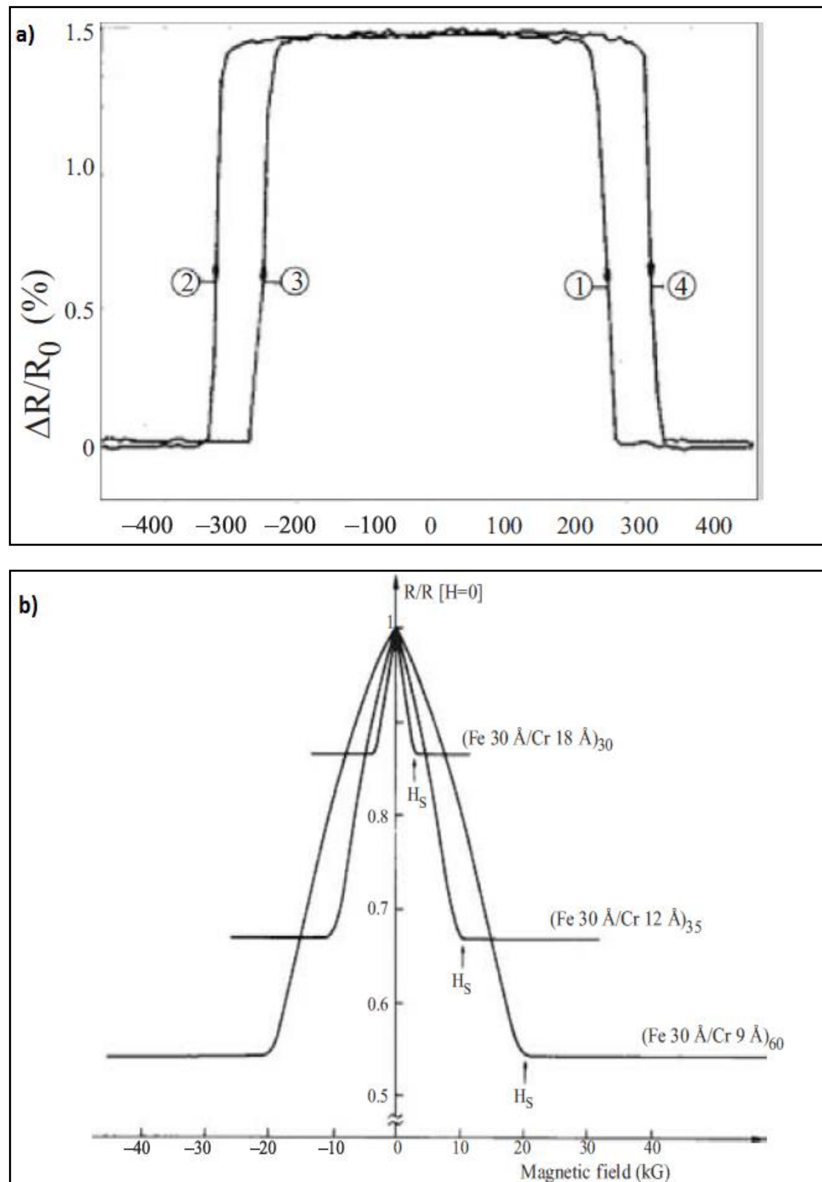

Figure 2.1: First observations of the giant magnetoresistance effect. a) MR data of Fe/Cr/Fe trilayers at room temperature b) MR measurements of Fe/Cr multilayers at 4.2 K.

The resistance of the system depends on the relative orientation of two ferromagnetic layers. If these magnetizations are parallel, the resistance of the system is at a minimum. If the magnetizations are antiparallel, the resistance of the system is at a maximum. This is called GMR effect. The MR can be defined as:

$$\mathrm{MR} = (\mathrm{R}_{\mathrm{AP}} - \mathrm{R}_{\mathrm{P}})/\mathrm{R}_{\mathrm{P}} \tag{2.1}$$

where R_{AP} is the resistance of antiparallel orientation (Figure 2.3 a) and R_P is the resistance of parallel alignment (Figure 2.3 b). It is common to employ two types of geometries to investigate GMR effect as shown Figure 2.2. The first one (Figure 2.2 a) is the current-in-plane geometry (CIP). In this geometry, the current flow is almost parallel to the interfaces of multilayer structure. The second geometry (Figure 2.2 b) is the current-perpendicular-to-plane geometry (CPP).

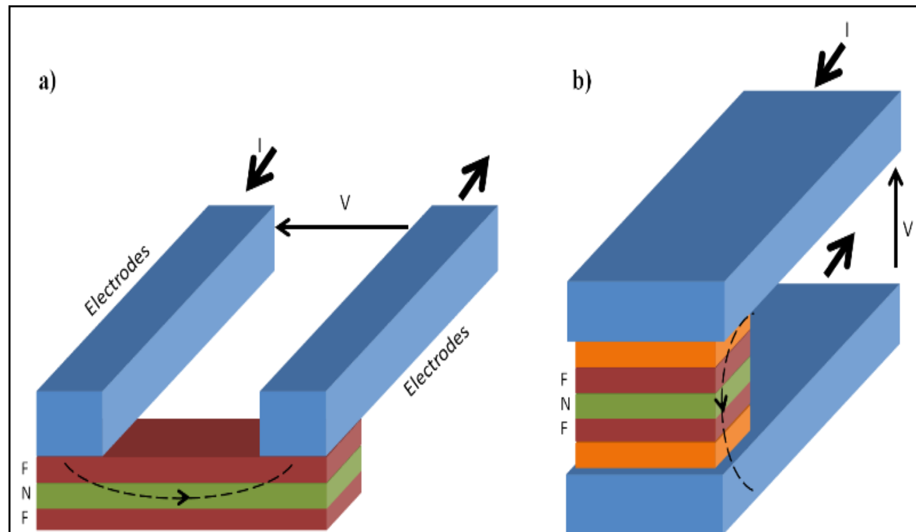

Figure 2.2: Geometries for GMR measurements. a) Current-in-plane (CIP) geometry and b) current-perpendicular-to-plane (CPP) geometry. Red layers correspond to F and green to N layers. Blue thick structures are electrodes (contacts) for measurements. Orange layers correspond to buffer and capping layers.

In this geometry, the current flows perpendicular to the interfaces. The CIP geometry is easier to realize since the CPP geometry needs to be prepared by lithographical techniques. In this thesis, nanolithographically defined samples in CPP geometry are used for GMR measurements. The nanofabrication processes were done in the cleanrooms of the Peter Grünberg Institute at the Jülich Research Center, Germany. In the coming sections nanofabrication process will be explained in details.

2.1.2.2. Physical picture of GMR effect

The GMR effect is simply explained with Mott's "Two current model" of conduction [13]. In 1936, Mott proposed that in ferromagnetic materials, conductivity can be defined as two independent channels, which correspond to the two spin orientation (up and down orientation) of the electrons. Spin-up and spin-down electron channels conduct in parallel and they don't mix with each other. On the other hand, spin-up and spin down electrons have unequal scattering ratios in ferromagnetic materials.

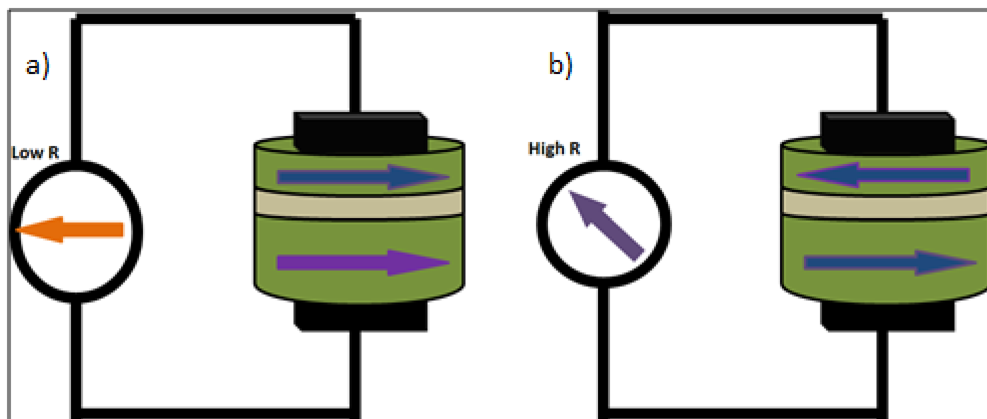

Figure 2.3: Illustration of GMR effect in CPP geometry. a) Antiparallel alignment (High Resistance) and b) parallel alignment (Low resistance). The arrows on the materials indicate direction of the magnetization of each magnetic layer.

Spin-up electrons will scatter less than spin-down electrons. This means the two channels have different resistivity values. In this model, it is important to emphasize that spin-flip scattering is neglected (thickness of thin film must be smaller than spin flip length). Using Mott's model to explain GMR effect, let's consider the system sketched in Figure 2.4. In Figure 2.4 a both layers' magnetizations are aligned parallel. Spin-up electrons will pass the multilayers weak scattering because the electrons' spins are collinear to the magnetization of both ferromagnetic layers.

In contrast, spin-down electrons will be scattered more strongly since their spin is antiparallel to both ferromagnetic layers' magnetizations. According to Mott's model, conduction will take place in both channels. Spin-up electrons

dominate in the conductivity, and the resistance of the system will be low. In other words, in P alignment one of the spin channels has low resistance compare to other one. If we consider the system in the antiparallel alignment in Figure 2.4 b, both (spin-up and spin-down) electrons will strongly scatter in one of the two F layers. Therefore, in AP alignment both channels have high resistance, and the resistance of the total system will be higher compared to the P alignment.

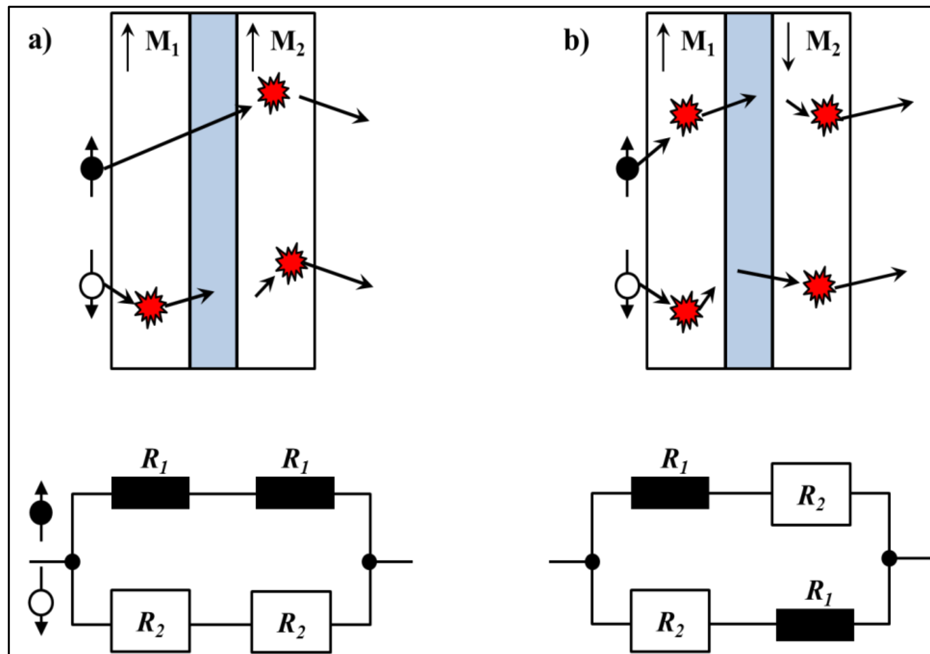

Figure 2.4: Two current model and corresponding to resistor model for a) parallel and b) antiparallel alignment of magnetic layers.

If we apply Mott's model to a resistor system, it is simple to obtain a quantitative description of the GMR value. (This model better fits in CPP geometry than CIP geometry). Let R_1 and R_2 correspond to resistance of spin-up and spin-down conduction channels in each magnetic layer. Then one can write the resistances for antiparallel (R_{AP}) and parallel (R_P) alignment as:

$$R_{AP} = \frac{1}{2}\,(R_1 + R_2) \tag{2.2}$$

$$R_P \; = \; 2R_1R_2/(R_1 + R_2) \tag{2.3}$$

From equations (2.2) and (2.3) one finds

$$R_{AP} = R_P + \frac{(R_1 - R_2)^2}{2(R_1 + R_2)} \tag{2.4}$$

From equation (2.4), it is clear that the resistance for the antiparallel alignment is larger than for the parallel alignment of magnetic layers. In other words, this means that the antiparallel alignment of the magnetic layers increases the resistance of the system. In asymmetric spin valves with F layers made from different materials the GMR value can be negative depending on the resistances $R_{1,2}^{left(right)}$ of the materials that are used for the left(right) F layer.

As it was mentioned in the beginning of this section, spin-flip scattering is not taken in account in Mott's Two Current Model. In 1993, Valet and Fert [14] proposed a theoretical model for the GMR effect including spin-flip scattering. In this model, Valet and Fert started from the Boltzmann equation to calculate magnetotransport properties of multilayer systems with CPP geometry. To understand the model, let's consider an F/N/F system with current flow from F to N to F. In the F layers, the current is spin-polarized (current densities of spin-up and spin-down electrons are not equal, in the F material the number of spin-up electrons is assumed to be larger than number of spin-down electrons). In the N material, however, spin-up and spin-down electrons are in balance. The question is what happens to spin-polarized current at F/N and N/F interfaces. At this interface there are more spin-up than spin-down electrons trying to penetrate into the N layer. Because of this spin accumulation, the electrochemical potentials for spin-up and spin-down electrons at the F/N interface deviate from their equilibrium values. Hence, the spin accumulation causes a potential difference at the interface that causes an additional resistance (boundary resistance) in the system. For the antiparallel alignment of the magnetizations of the F layers, the system will have larger amount of spin accumulation, and this will give rise to a larger resistance of the system. For parallel alignment of the F layers, the amount of spin accumulation will be less than for the antiparallel alignment of F layers. This means that antiparallel alignment will have a larger system resistance than parallel alignment. The extent of the spin accumulation from the interface depends exponentially on spin diffusion length.

When the spin diffusion length increases, spin accumulation decreases faster. For this reason the spin diffusion length is a key parameter of CPP-GMR.

2.1.3. Tunnel magnetoresistance (TMR)

Although tunnel magnetoresistance (TMR) effect was not investigated in this thesis, I will give a short summary about TMR. TMR is observed in magnetic tunnel junctions (MTJ). MTJs are multilayers that consist of two ferromagnetic layers separated by a thin insulating layer. The main physical difference between GMR and TMR is the spacer layer between the ferromagnetic materials. As described above, in GMR, there is nonmagnetic metallic spacer layer but in TMR, this nonmagnetic metallic layer is replaced with a very thin insulator, which forms a so called tunnel barrier. Conduction through the tunnel barrier depends on quantum mechanical tunneling. Spin dependent tunneling is the main reason of TMR. Similar to GMR, the resistance of the system is lower when the F layers are parallel compared to the resistance of the system when the FM layers are antiparallel. Today, the maximum experimentally observed value of TMR is one to two orders of magnitude larger than than the maximum GMR value.

The first TMR effect was observed in 1975 by Jullière. He observed a change in the resistance in Fe/Ge/Co multilayers at 4.2 K [15]. After the discovery of the GMR effect and with the improvement in deposition techniques, which are required for growing a few nanometers thick tunnel barriers, in 1995, larger TMR effects were observed in Fe/AlO_x/Fe multilayer systems at room temperature [16],[17]. In the 2000s, MgO was started to be used as an insulator between the ferromagnetic layers, and around 200% of MR was achieved at room temperature [18],[19]. The TMR effect is explained by the Jullière model [15] in simple way. This model is similar to Mott's two current model. Derivations were done without taking spin-flip tunneling into account in a similar way like for the GMR effect. Majority and minority electrons don't have equal tunneling probability. That is, when the magnetizations (spins) of both ferromagnetic layers are parallel, the majority electrons in one layer will easily tunnel to majority band in the second layer while

the minority electrons in the first layer tunnel to the minority states in the next layer. For the case of antiparallel alignment, the majority electrons has to flip to be parallel of the second layer spins in order to be accepted by the second layer. This spin flip means scattering of the tunneling electrons by the magnetic moments of the second layer (minority in this case). Thus the electrical resistivity becomes larger compared to that for parallel case.

2.1.4. Spin transfer torque (STT)

Spin transfer torque is the interaction of a spin-polarized current with the local magnetization in a ferromagnet. Magnetic moments are transferred from the conduction electrons to the magnetization, and this transfer change of the magnetization orientation because of the conservation of spin angular momentum. In other words, when a spin-polarized current passes through a ferromagnetic material, some part of the spin angular momentum that is carried by conduction electrons is transferred to local electrons in the ferromagnet. In classical mechanics, change of angular momentum per unit time is equal to a torque, so one can conclude that the spin-polarized electrons can apply a torque directly to the magnet.

2.1.4.1. Historical background and prior works

The history of STT is older than the discovery of GMR. In 1984, L. Berger published an article [20] about the relation between conduction electrons and local electrons. Several similar studies were done in that decade [21], [22], [23]. During that time experimental studies were also done, but micro- and nanofabrication techniques were not sufficient to prepare ideal (small enough) samples for the investigations. The main obstacle was that STT requires high current densities; to provide this and to keep the sample alive, small conduction cross-sections are needed. However, at that time microfabrication techniques were not sufficiently matured for the preparation of such samples. In 1996 Berger and Slonczewski,

separately, predicted that a spin-polarized current could transfer some of its magnetic moment to the magnetization of a ferromagnetic material through which the current is passing [4],[5]. These publications by Berger and Slonczewski received great attention. Two years later, in 1998, Tsoi et al. [6] reported magnetic excitations caused by a current of high density injected through a point contact into a Cu/Co multilayer (Figure 2.5).

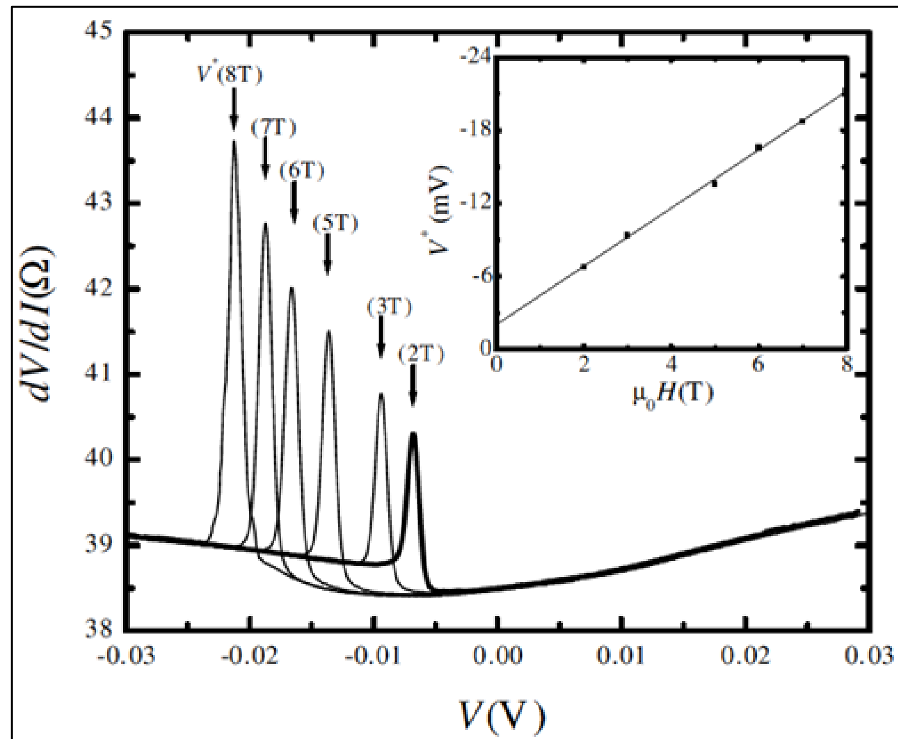

Figure 2.5: Magnetic excitations in a Co/Cu multilayer due to a current injected through a point contact .

In 1999, Myers et al. [8] observed magnetic excitations by passing current through a Co/Cu/Co sandwich structure in a lithographically prepared a Silicon Nitride membrane (Figure 2.6). In addition to magnetic excitations, they also observed current-induced magnetic switching. In the same year, magnetic excitations have been reported by Wegrowe et al. in an electroplated Ni wire [24], and by Sun in manganite junctions [7]. In 1999 was the year when STT became one of the hot topics in magnetism. One year later, at the beginning of the new millennium, Katine et al. [10] observed STT-induced magnetization reversal in a Co/Cu/Co spin-valve nanopillar structure (Figure 2.7).

Diameter of the nanopillar was about 100 nm and they used GMR effect as a probe for magnetization reversal. It was the first STT experiment done on nanofabricated nanopillars. After 2000, theoretical and experimental studies on STT have grown rapidly.

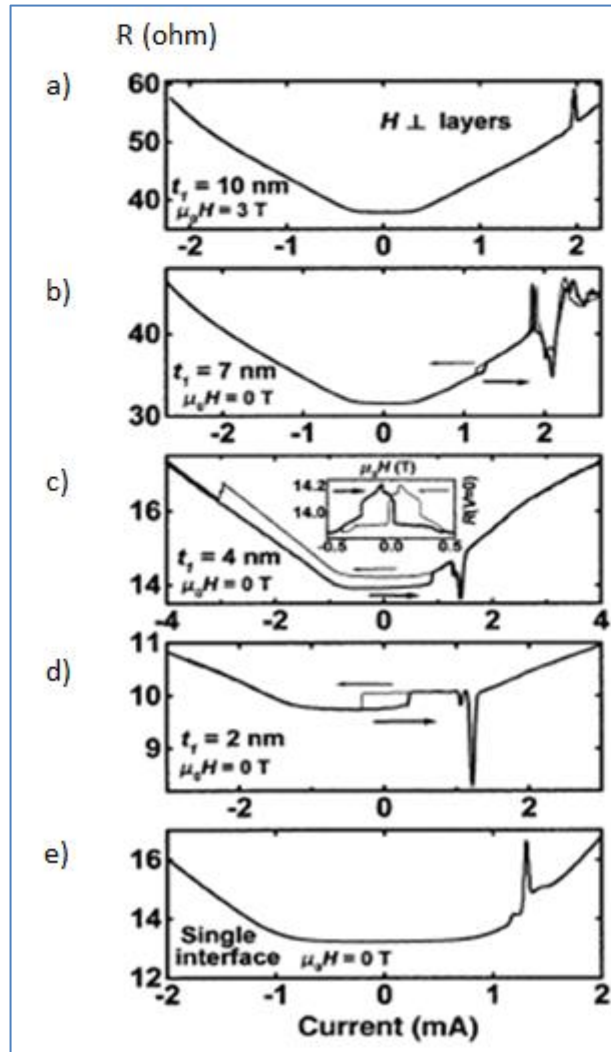

Figure 2.6: Magnetic excitations and current-induced magnetization switching observed by the Cornell group. Resistance values of thin Co layer for a) 10 nm b) 7 nm c) 4 nm d)2 nm e) single interface.

STT effect has been also studied in different devices and geometries. But up to 2004, spin valve structure that has been investigated was consisting of two ferromagnetic layer separated by thin nonmagnetic metal layer. In 2004, both Grandis Corporation and Cornell group showed magnetic reversal induced by spin

transfer torque in nanoscale magnetic tunnel junctions (MTJ) with very thin AlOx tunnel barriers [25], [26].

After those, similar works were also done with MgO tunnel barriers. In addition to those works, spin transfer torque has been used to manipulate domain walls in magnetic nanowires [27], [28], [29]. Today, STT became commercial product as spin transfer torque magnetic random access memory (STT MRAM). STT MRAM is one of the important candidates as RAM of future computers, smartphones and solid state drives. STT MRAM is commercial product nowadays.

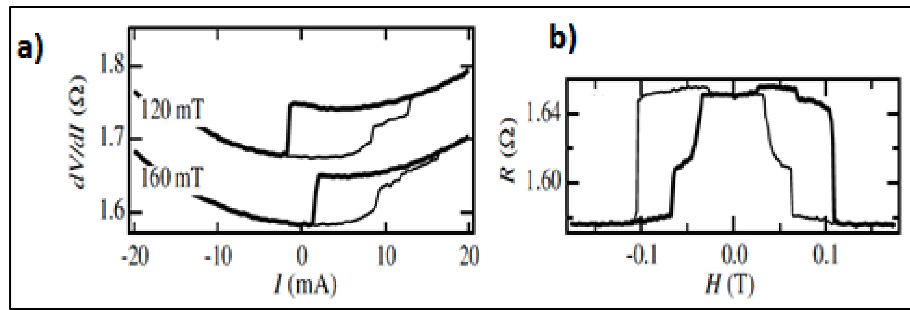

Figure 2.7: Current-induced magnetization switching in Co/Cu/Co nanopillars. a) Switching by current b) GMR measurements with same nanopillar structure.

2.1.4.2. Theoretical background

In this part of the chapter, we will have a look into the mechanism underlying the spin transfer torque effect. To make it easy first, we will consider that one electron with a given spin orientation is travelling from a non-magnetic metal to a ferromagnetic layer. As it can be seen from Figure 2.8 the magnetization of the magnetic layer is in the **z** direction, and electron is propagating in the **x** direction. The electron's spin direction is given by an angle θ in the **xz** plane. (These coordinates are chosen to make the primitive spin transfer torque picture understandable. Otherwise STT and STO with perpendicular magnetic anisotropy are investigated and also used in STT-MRAM structures). Obviously the magnetization of the ferromagnet and electron spin is not collinear. From quantum mechanics, the electron spinor state can be written as $\begin{pmatrix} \cos\frac{\theta}{2} \\ \sin\frac{\theta}{2} \end{pmatrix}$. Hence, it is the

superposition of spin-up and spin-down states with respect to the quantization axis defined by the magnetization in the ferromagnet. Spin-up and spin-down components are represented by $\begin{pmatrix} \cos\frac{\theta}{2} \\ 0 \end{pmatrix}$ and $\begin{pmatrix} 0 \\ \sin\frac{\theta}{2} \end{pmatrix}$, respectively. When the electron reaches the interface between the magnetic layer and the non-magnetic layer, first, the interface can act like a spin filter. For our simplified consideration we assume a perfect spin filter: Spin-up electrons continue into the magnetic layer, but spin-down electrons are reflected. As it can be seen, the transverse component (given by$\sin\theta$) is absorbed by the ferromagnetic layer. This was for one electron. If many electrons are taken to account, for a thin enough ferromagnet, sufficient amount of current can be passed to apply a torque to re-orient the direction of the magnetization. Now, if we consider a system with two magnetic layers separated by a non-magnetic layer, then the situation becomes interesting. This separation layer can be non-magnetic metal or a very thin insulator. One of the magnetic layers is thinner than the other magnetic layer. In fact, it is harder to switch the thicker one. The thick layer will be called “fixed (pinned)” layer and the thin one will be called “free” layer. It is important to assume that the magnetizations of the two magnetic layers are misaligned by a small angle, e.g. due to thermal excitation.

Now let’s consider that electrons are flowing from fixed layer to free layer (left part of Figure 2.8). They will reach the free layer with their spin aligned in the direction of fixed layer. When they penetrate into the free layer, they will exert a torque by transmitting their transverse component of angular momentum. In order to conserve the total angular momentum, the free layer will tend to align its magnetization parallel to the incoming electrons.

In other words, this torque on the free layer will push the free layer to re-orient its alignment parallel to the fixed layer’s orientation. If the current is sufficient strong, they will be in parallel orientation.

In the opposite case (right part of Figure 2.8), when the electrons flow from the free layer to the fixed layer, they will be polarized in the direction of free layer. When they reach the fixed layer, they will exert a torque on the fixed layer. But it will be not sufficient to re-orient the fixed layer’s magnetization. Most importantly, electrons with a spin momentum antiparallel to the fixed magnetization will be

reflected from fixed layer (spin filtering). They will return to the free layer and push the free layer to re-orient to become antiparallel to fixed layer.

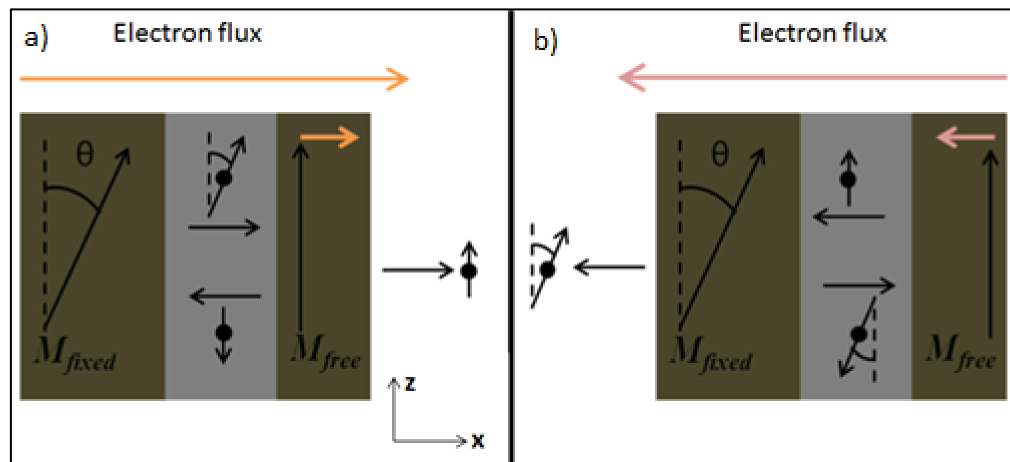

Figure 2.8: Physical picture of the STT effect for the two directions (long horizontal arrows) of electron flux. Direction of electron flux is a) from thick to thin layer b) thin to thick layer.

Hence, depending on current direction and magnitude, a spin-polarized current can align two magnetic layers parallel or antiparallel to each other. This is called current-induced magnetization switching. This phenomenon is the main principle of the STT-MRAM. By current-induced magnetization switching, external magnetic fields are replaced by current to manipulate the magnetization orientation (Figure 2.10). This has many advantages as compared to conventional RAMs. A review will be given in coming sections about STT MRAM.

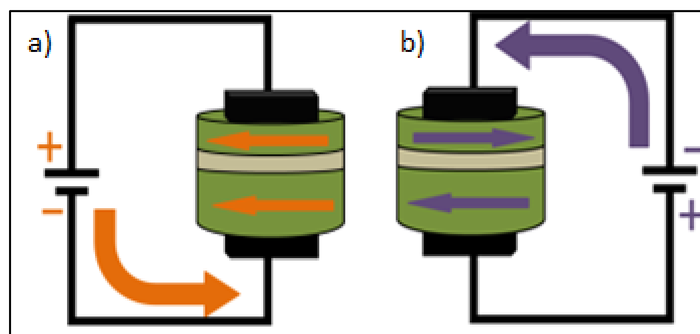

Figure 2.9: Current-induced magnetization reversal. Current flows from a) thick layer to thin layer b) thin layer to thick layer.

Stiles and Zangwill proposed a more rigorous quantum mechanical treatment of the spin transfer torque effect [30], [31] that I will briefly summarize in the following. Let's consider a multilayer system that consists of two ferromagnetic layers separated by a non-magnetic layer with their magnetizations misaligned by an angle θ as mentioned above.

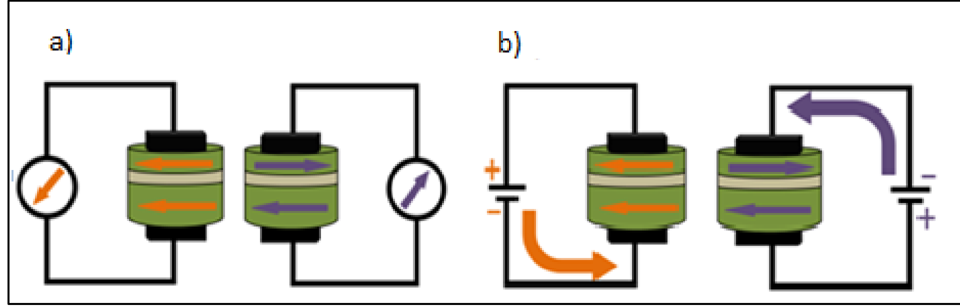

Figure 2.10: Comparison of GMR vs. STT. a) GMR circuit b) STT circuit.

As before, the wave function of an electron is written as superposition of spin-up and spin-down components,

$$\psi_{in} = \frac{e^{ikx}}{\sqrt{\Omega}} \left[\cos\left(\frac{\theta}{2}\right)|\uparrow\rangle + \sin\left(\frac{\theta}{2}\right)|\downarrow\rangle\right] \tag{2.5}$$

where Ω is normalization volume. According to their spin states electrons will be subjected to different potentials $V_\uparrow$ and$V_\downarrow$, respectively, and $V_\downarrow$ = $V_\uparrow$ +Δ, where Δ is the exchange energy. We can assume incoming electron has energy of $E = \hbar^2/2mE$, wave vector of $k = \sqrt{2mE}/\hbar$ and outside of ferromagnet wave vectors $k_\uparrow = k$ and $k_\uparrow = \sqrt{2m(E-\Delta)}/\hbar$ where$E > \Delta$. For simplicity, if we take $V_\uparrow$ =0 and according to the required continuity of the wave functions at the interface, reflected and transmitted wave functions can be written as:

$$\psi_{trans} = \frac{e^{ik_\uparrow x}}{\sqrt{\Omega}} \cos\left(\frac{\theta}{2}\right)|\uparrow\rangle + \frac{e^{ik_\downarrow x}}{\sqrt{\Omega}} \frac{2k}{k+k_\downarrow} \sin\left(\frac{\theta}{2}\right)|\downarrow\rangle \tag{2.6}$$

$$\psi_{ref} = \frac{e^{-ikx}}{\sqrt{\Omega}} \frac{k-k_\downarrow}{k+k_\downarrow}\left[\sin\left(\frac{\theta}{2}\right)|\downarrow\rangle\right] \tag{2.7}$$

The spin current density is formulated as:

$$\boldsymbol{\Phi} = \frac{\hbar^2}{2m} Im(\psi^* \sigma \otimes \boldsymbol{\nabla}\psi) \tag{2.8}$$

where, σ is the Pauli matrix. Writing the spin current densities of incident, reflected, and transmitted wave functions by using equations (2.6), (2.7) and (2.8) we get

$$\boldsymbol{\Phi_{in}} = \frac{\hbar^2}{2m\Omega}(kcos\theta\boldsymbol{x} + ksin\theta\boldsymbol{y}) \tag{2.9}$$

$$\boldsymbol{\Phi_{ref}} = \frac{\hbar^2}{2m\Omega} k \left(\frac{k - k_\downarrow}{k + k_\uparrow}\right)^2 \left(\sin\frac{\theta}{2}\right)^2 \boldsymbol{z} \tag{2.10}$$

$$\boldsymbol{\Phi_{tran}} = \frac{\hbar^2}{2m\Omega} ksin\theta(\cos[(k_\uparrow - k_\downarrow)x]\boldsymbol{x} - sin[(k_\uparrow - k_\downarrow)x]\boldsymbol{y}) \\ \frac{\hbar^2}{2m\Omega}\left[k\left(cos\frac{\theta}{2}\right)^2 - k_\downarrow\left(\frac{2k}{k + k_\uparrow}\right)^2\left(\sin\frac{\theta}{2}\right)^2\right]\boldsymbol{z} \tag{2.11}$$

According to conservation of angular momentum, the total momentum on the left ($\boldsymbol{\Phi_{in}} + \boldsymbol{\Phi_{ref}}$) and right ($\boldsymbol{\Phi_{tran}}$) side of the interface must be equal. But as it is seen they are not equal. The "missing" part is transmitted to the ferromagnetic layer. The torque that is applied to magnetization of the ferromagnetic layer is then given as:

$$\boldsymbol{\tau} = A(\boldsymbol{\Phi_{in}} + \boldsymbol{\Phi_{ref}} - \boldsymbol{\Phi}_{tran}) \tag{2.12}$$

where A is the area of F/N interface. With the expressions of the spin current densities in equations (2.9) to (2.11) the torque exerted to FM layer becomes

$$\boldsymbol{\tau} = \mathrm{A}\frac{\hbar^2 \mathrm{k}^2}{2\mathrm{m}\Omega} sin\theta(\cos[(k_\uparrow - k_\downarrow)x]\boldsymbol{x} + sin[(k_\uparrow - k_\downarrow)x]\boldsymbol{y}) \tag{2.13}$$

As it is seen, when the spin-polarized current enters ferromagnetic layer from a non-magnetic layer, it loses angular momentum. This lost angular momentum is transferred to the magnetic layer as torque. This is spin transfer torque. If the angle between magnetizations of magnetic layers (θ) is 0 or π, then the torque is also equal to 0.

2.1.4.3. Geometries for STT

As mentioned in historical background section, there are several geometries that are employed to investigate STT measurements. In all device geometries, the main aim is to fabricate devices in which the electrical current flows in a small. The first reason is the reduction of the current needed to manipulate layers with volume. By keeping the free layer's volume small, the number of total magnetic moments, which are to be manipulated, is reduced. High currents also cause a heating problem. If the sample's temperature increases too much, it will cause additional effects inside the sample. In the worst case, the sample will be destroyed.

Second reason is that for small cross-sections the STT is dominant over the magnetic field generated by current (Oersted field). The circular magnetic field generated by the current tends to produce vortex-type magnetization states instead of magnetization reversal. If we consider a nanopillar device as a wire of diameter d, the Oersted field at the wire surface scales like I/d, whereas the strength of the STT scales like the current density, I/d^2. Obviously, for diameters less than a critical value (about 1 μm) the STT effects will dominate over the Oersted field.

As it is seen in Figure 2.11, adapted from [32], there are more or less 6 types of device geometries used in literature for STT experiments. In Figures 2.11 (a) and (b), the device is a mechanical point contact to a multilayer or single ferromagnetic layer. The point contact to multilayer device is the first geometry used in STT experiments by Tsoi et al. [5], see Figure 2.5. A peak of differential resistance is observed in one polarity of current.

A sharpened wire tip is gently pressed to the sample, and the contact area can be calculated from the resistance. Mechanical point contacts have some advantages

over lithographically defined systems. They are relatively easy to produce, and the shape and place that the tip contacts are not so critical when compared to lithographically fabricated devices.

In Figures 2.11 (d) and (e) lithographically fabricated point contact devices are shown. Mechanical point contact devices were easy to fabricate but the adjustment of the contact area was still a big issue for STT experimentalists. Since tips are sensitive and very small, so they could be broken after several measurements. To overcome this issue lithographically point contacts were developed and first lithographically point contact experiments were done by Myers et al. [8], Figure 2.7.

By means of electron beam (e-beam) lithography and reactive ion etching techniques, a hole is made in an insulator layer (Si_3N_4) on the top of a multilayer. The desired material for the point contact is finally deposited on the top of insulator layer. Lithographically defined point contacts need more work than mechanical point contacts but they are not as fragile as mechanical point contacts.

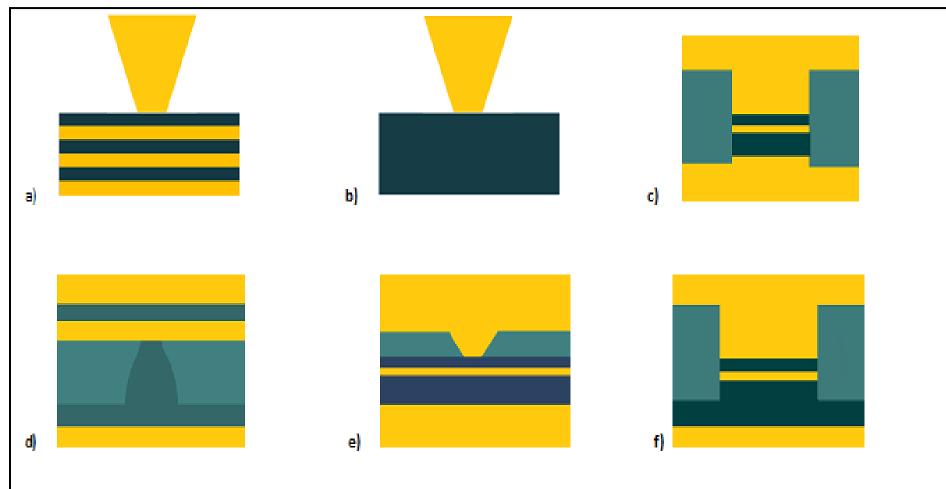

Figure 2.11: Nanofabricated geometries for STT experiments. a) multilayer point contact, b) single layer point contact , c) nanopillar (lithographically fabricated), d) lithographically fabricated point contact to single layer, e) lithographically fabricated point contact to multilayer, and f) nanopillar with extended fixed layer (lithographically fabricated). Dark (light) layers are ferromagnetic (non-magnetic).

Lithographically fabricated nanopillar devices (Figure 2.11 c and f) are widely used in STT experiments. They have several advantages over point contact devices. For instance, they require less current density than point contacts. In nanopillar

devices, it is easier to control the magnetic properties of free and fix layers since they restricted to small areas.

Nanopillars are properly suited to the theoretical work described by Berger and Slonczewski in references [4], [5]. The first nanopillar device was nanofabricated by Katine et al. [10], as in Figure 2.6. As mentioned above a Co/Cu/Co nanopillar multilayer was fabricated. There are two methods of nanopillar device patterning: additive and subtractive patterning. In this work, as it will be widely explained in next chapter, subtractive patterning is applied to the raw sample stack. It is important to mention that it is more difficult fabricate nanopillar structures than the other structures shown in Figure 2.11.

2.1.4.4 Current-induced magnetization dynamics

Magnetization dynamics in the presence of spin transfer torque can be described within the Landau-Lifschitz-Gilbert (LLG) equation by introducing an additional spin transfer torque term (Slonczewski term). If the LLG equation of magnetization dynamics is applied to the magnetization vector representing the complete ferromagnetic layer, it gives a solution in macrospin approximation.

The torque ($\overrightarrow{T}$) applied by an effective magnetic field ($\overrightarrow{H}$) to the magnetic moment ($\overrightarrow{\mu}$) is formulated by:

$$\overrightarrow{T} = \overrightarrow{\mu} \times \overrightarrow{H} \quad (2.14)$$

This torque is also equal to change in the spin angular momentum with respect to time:

$$\frac{d\overrightarrow{S}}{dt} = \overrightarrow{T} = \overrightarrow{\mu} \times \overrightarrow{H} \quad (2.15)$$

The magnetic moment can be quantum mechanically be expressed as:

$$\vec{\mu} = \frac{-g\mu_B}{\hbar}\vec{S} \qquad (2.16)$$

If one combines (2.15) and (2.16), the dynamics of the magnetic moment of an electron can be written as:

$$\frac{d\vec{\mu}}{dt} = -\gamma\vec{\mu} \times \vec{H} \qquad (2.17)$$

where $\gamma = {g\mu_B}/{\hbar}$ is the gyromagnetic ratio. For the total volume, equation (2.17) yields

$$\frac{d\vec{M}}{dt} = -\gamma\vec{M} \times \vec{H} \qquad (2.18)$$

The $(-\gamma\vec{M} \times \vec{H})$ term means that the magnetization precesses around the applied magnetic field $(\vec{H})$. However, it doesn't precess forever. After a while the magnetization aligns parallel to $\vec{H}$. Hence, there must be a damping term in this equation. According to theory of Gilbert (Gilbert's PhD Thesis in 1956), this term must be proportional to ${d\vec{M}}/{dt}$. And then equation (2.18) becomes

$$d\vec{M}/dt = -\gamma\vec{M} \times \vec{H} + \frac{\alpha}{M_s}\vec{M} \times \frac{d\vec{M}}{dt} \qquad (2.19)$$

Equation (2.19) is called Landau-Lifschitz-Gilbert (LLG) equation. In this equation α is Gilbert damping constant. The first part of the equation is the precession term (gyromagnetic motion) and the second part describes damping, which aligns the magnetization along the effective field axis. If we divide both sides by M_s (saturation magnetization) and substitute $d\vec{m} = {d\vec{M}}/{M_s}$ we get:

$$\frac{d\vec{m}}{dt} = -\gamma\vec{m} \times \vec{H} + \alpha\vec{m} \times \frac{d\vec{m}}{dt} \quad (2.20)$$

According to Slonczewski [5] the torque applied to free layer by the spin-polarized current can be written as:

$$\frac{d\vec{m}_{free}}{dt} = \frac{I}{A} g(\theta)\vec{m}_{free} \times \left(\vec{m}_{free} \times \vec{m}_{fixed}\right) \quad (2.21)$$

In this equation $I/_A$ is current density, $g(\theta)$ is the material-, polarization-, and angle- (between free and fixed layers' magnetizations) dependent STT efficiency. If we add this so called Slonczewski term to equation (2.20) then we get the Landau-Lifschitz-Gilbert- Slonczweski (LLGS) equation

$$\frac{d\vec{m}_{free}}{dt} = -\gamma\vec{m}_{free} \times \vec{H} + \alpha\vec{m}_{free} \times \frac{d\vec{m}_{free}}{dt} + \frac{I}{A} g(\theta)\vec{m}_{free} \left(\vec{m}_{free} \times \vec{m}_{fixed}\right) \quad (2.22)$$

According to the LLGS equation, depending on the direction of the current, the Slonczewski term can either increase or decrease the effective damping in the system (Figure 2.12). In other words, depending on the direction of the current, when STT and damping vectors are in the same direction, STT stabilizes the present alignment between fixed and free layer. In contrast, when the STT and damping vectors are antiparallel, the STT forces the free layer to switch with respect to the fixed layer.

In Figure 2.13, Extracted from [31], simple scenarios for current-induced magnetization dynamics are depicted. In Figure 2.13 a, the damping torque is larger

than STT. Hence, the magnetization of free layer relaxes towards the applied field (low current and high field case). In Figure 2.13 b, the STT is larger than damping torque and leads to current-induced magnetization switching (high current case). In Figure 2.13 c, the damping torque is equal to the STT. In this case energy losses due to damping are exactly compensated by energy supply from the applied current and steady oscillations of the magnetization around the effective field axis are observed (matching of high current with applied field). The oscillation frequency is roughly of the order of the ferromagnetic resonance (FMR) frequency.

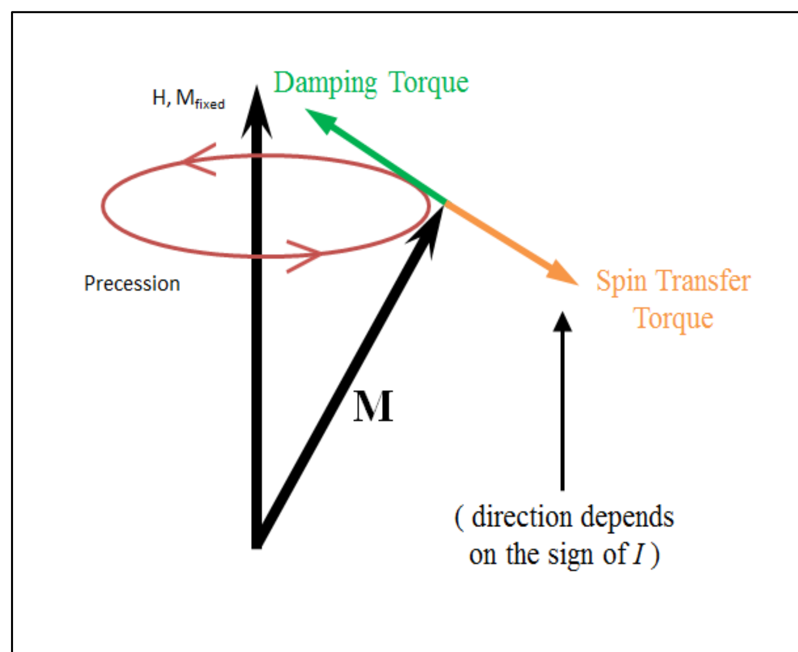

Figure 2.12: Torques in current-induced magnetization dynamics. Spin transfer torque's direction depends on the direction of the current, either parallel or antiparallel to the damping torque. The latter case is shown in the figure.

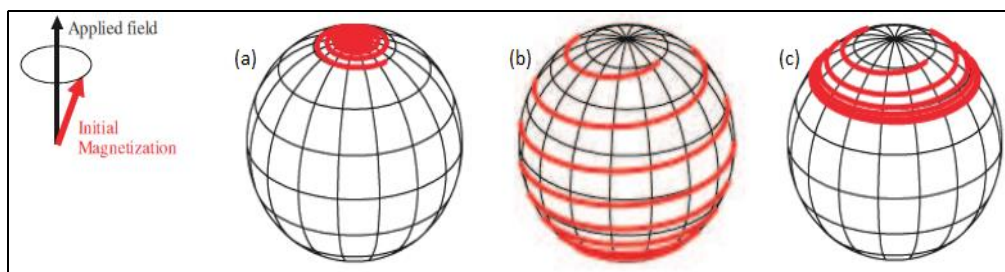

Figure 2.13: Current-induced magnetization dynamics when a) the magnetization of free layer relaxes towards the effective magnetic field, b) the magnetization switches (here from north to south pole), and c) the free layer magnetization steadily oscillates around the effective magnetic field.

2.1.5. Spin transfer oscillators (STO)

As mentioned above, when there is balance between damping torque and STT, the magnetization of the free layer starts to precess in steady state [9]. As a result the angle between the fixed and free layer magnetizations periodically varies. By virtue of the GMR (or TMR) effect, the resistance of the system also varies periodically and, thus, the applied DC current generates a radio frequency (RF) voltage signal. This configuration is called spin transfer oscillator (STO). The output RF can be tuned via the applied magnetic field and the DC current magnitude in a range typically between one to tens of GHz. Summarizing, an AC voltage is produced by a DC current in a nanoscale device. This makes STOs ideal candidates for microwave circuits.

STOs have many advantages over traditional voltage-controlled oscillators. They can be tuned by current and magnetic field. They have very small size and simple structure. Because of this simplicity, they can be easily integrated into today's silicon technology and production costs are less compare to other chip oscillators. Furthermore, their energy consumption is less than that of conventional oscillators, and they are working in wide temperature range. All these advantages make STO promising candidate for chip-to-chip communications, wireless communications, microwave sensors and other microwave applications. However, there are some challenges to be overcome. For instance their output power is still inadequate and linewidth of the oscillation has to be reduced to make STOs attractive for practical use in industrial applications. Strategies to achieve such improvements can be found in [33].

2.1.6. STT magnetic random access memory (STT-MRAM)

The spin transfer torque magnetic random access memory (STT-MRAM) is a new type of magnetic random access memory that is a promising candidate for future information technologies. Before explaining the working principle of STT-

MRAM, I will give a brief introduction about magnetic random access memories (MRAM).

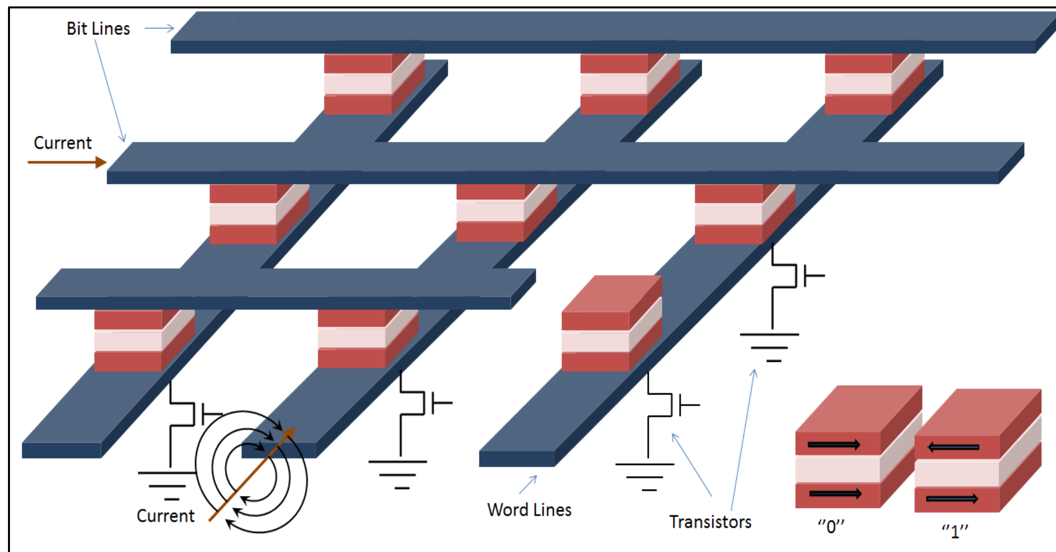

Figure 2.14: Cross-point architecture for an MRAM array.

MRAM is a solid state RAM that employs magnetic tunnel junctions. In MRAMs bits are stored by the magnetization alignment of magnetic layers: parallel or antiparallel to each other (Figure 2.14). The writing process in a single bit cell is done by passing current through the appropriate pair of the bit and word lines. In this case transistor is off. These currents generate Oersted field, which add up at the position of the MTJ to be writing and changes the magnetization direction of the free layer in only this MTJ. But in array of MTJ structures, applied current also affect the other MTJ cells (half selection problem). To overcome this issue, toggle MRAM was proposed in 2006 by Everspin [35]. For the reading process the GMR or TMR effect is exploited. When parallel alignment of magnetic layers occurs, the resistance is low corresponding to “0”, whereas antiparallel alignment yields a high resistance corresponding to “1” (Figure 2.14).

In order to select only one MTJ of the whole array for the readout, a transistor (not shown in the figures) needs to be placed in series with each MTJ. The transistor is off for the writing process, but on for the bit selection during the reading.

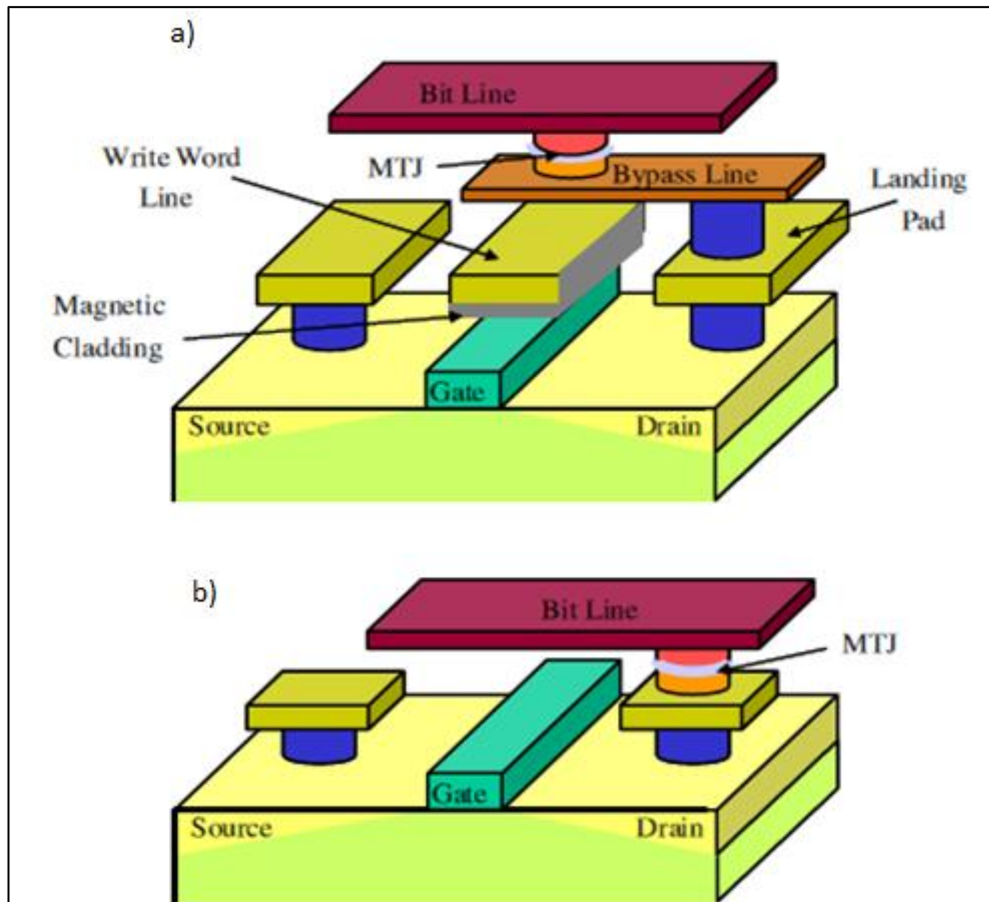

Figure 2.15: Prototype of a) the conventional MRAM configuration and b) the STT-MRAM configuration. Note, that the volume occupied by the STT-MRAM is less than for the conventional MRAM.

In STT-MRAM, the magnetization of the free layer is switches by a spin-polarized current as discussed in the description of theory of spin transfer torque. In this way, the half selection problem is solved (Figure 2.15, Extracted from [33]), since the current generating the STT flows through only one MTJ. Hence, in STT-MRAM the bit line is not required; instead the current passes through the MTJ. Spin transfer torque is new mechanism to write the bit cells, which has the potential to reduce the size and also the energy consumption of the cell.

2.2 Heusler alloys

Heusler alloys constitute a large material family with more than 1500 members. These alloys were first discovered in 1903 by the German mining

engineer and chemist Friedrich Heusler [35],[36]. He found that Cu_2MnAl was showing ferromagnetic behavior without containing a ferromagnetic element. In 1929 Potter [37] and in 1934 Bradley and Rodgers [38] investigated the structural properties Cu_2MnAl via X-ray diffraction methods. They established the relation between structure and physical properties. The discovery of Heusler alloys opened new horizons in material science, chemistry, and physics.

Although they are known for more than a century, in recent years new Heusler alloys and new properties of them were discovered. These alloys attracted great attention because of their wide range of physical properties, such as half metallic ferro- and ferrimagnetism [39],[40], topological insulating behavior [41], [42], [43], or multiferroism [44],[45]. All these properties make them important candidates especially for spintronics and other nanoelectronic applications [46].

There are two classes of ternary Heusler alloys. The first group are the half Heusler alloys XYZ with an elemental ration X:Y:Z = 1:1:1. The second group is the full Heusler alloys, which have the chemical composition X_2YZ (2:1:1). In these formulas X and Y are transition metal group elements, and Z is a III-V group elements. Chemically, full Heusler alloys have the $L2_1$ and half Heusler alloys the $C1_b$ structure.

In 1983, de Groot and his colleagues [47] predicted half metallic ferromagnetic behavior of NiMnSb using band structure calculations. This material was experimentally investigated by Park in 1998 [48]. Half metallicity describes different behavior of the material for the two different spin states. For spin-up electrons, half metallic ferromagnetic materials behave as a conductor, but for spin-down electrons as a semiconductor or an insulator. This leads to 100% spin polarization at the Fermi level, which is expected to increase the efficiency of magnetotransport phenomena such as GMR, TMR, and STT (Fig.2.16). As mentioned above in the theory and description of spin transfer torque, high spin polarization is important condition for magnetization switching and dynamics induced by spin-polarized currents. Half metallic ferromagnetic behavior makes half metallic ferromagnets important candidates for spintronic and other applications.

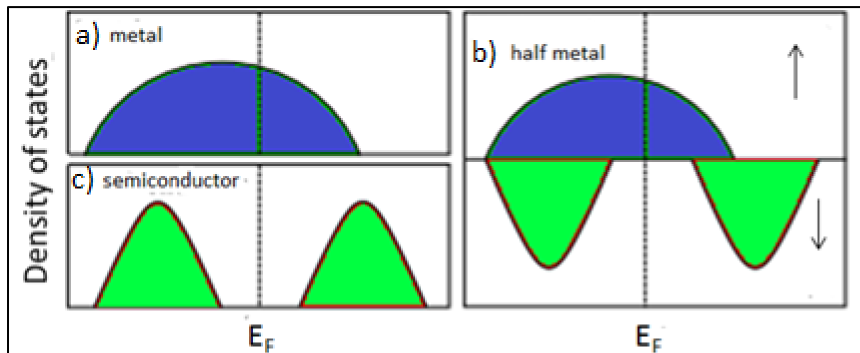

Figure 2.16: Comparison of the density of states of a) metal, b) a half metal c) semiconductor.

Because of its physical and structural properties (high spin polarization, high Curie temperature, etc.), Co_2MnSi is one of the promising candidates for future spintronic applications. Co_2MnSi is a full Heusler alloy and has $L2_1$ type structure (Figure 2.17). This Heusler alloy was theoretically investigated by Ishida et al. [49] and found to be a half metallic ferromagnet. His work attracted great attention.

Compared to other full Heusler alloys, Co_2MnSi has a higher Curie temperature of 985 K, which is an important condition for spintronic devices [50] that are working at or above room temperature.

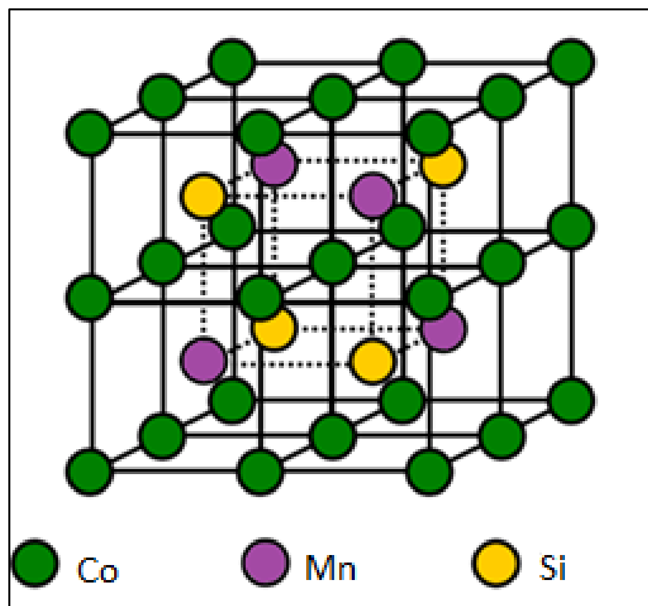

Figure 2.17: $L2_1$ structure of the Co_2MnSi Heusler alloy.

The second important condition for spintronics applications is the experimental spin polarization value. Experimental results of point contact Andreev reflection spectroscopy showed that Co_2MnSi (for bulk and thin film) has around 60% spin polarization [52], [53], [54], [55], [56]. For comparison, Fe, Co and Ni have spin polarization about 51% at low temperature [57]. Hence, the spin polarization of Co_2MnSi is higher than those of the ferromagnetic 3d elements. From Figure 2.18, it can be seen that Co_2MnSi behaves like insulator in the spin-down channel and like conductor in the spin-up channel.

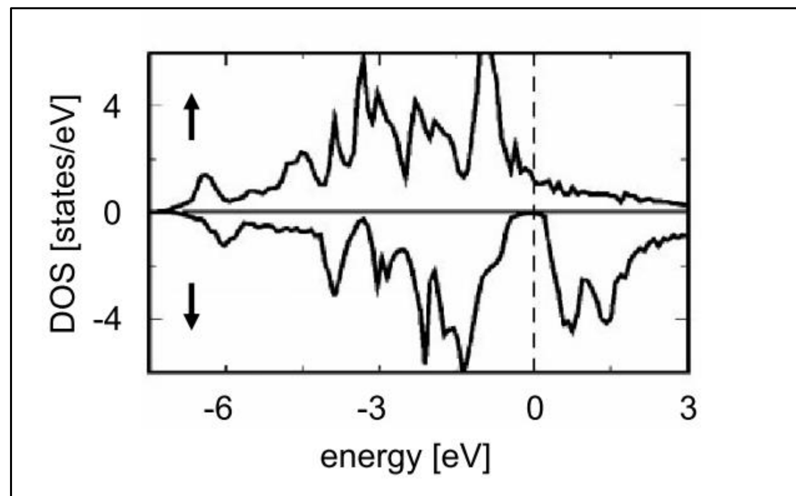

Figure 2.18: Density of states for Co_2MnSi. The spin-split band structure, insulating behavior for spin-down electrons of Co_2MnSi.

3. EXPERIMENTAL TECHNIQUES

This chapter is divided into two parts. In the first part, we focus on the nano-fabrication techniques and sample preparation. The second part is dedicated to measurement techniques and the set-up that is used during experiments. The work described below was made in the 10-100 class clean rooms of the Peter Grünberg Institute at the Jülich Research Center. The description of the nanofabrication process is mostly adapted from the article: "*Charging effect reduction in electron beam lithography and observation of single nanopillars on highly insulating substrates*" by Şaban Tırpancı, Daniel E. Bürgler, Claus M. Schneider, Bulat Rameev, and Bekir Aktaş that was published in the journal *Microelectronic Engineering* [59].

Nanofabrication is very interesting and important interdisciplinary branch of science that is today widely used in many research disciplines (from biology to electronics) and industry. This field is based on the curiosity of scientists about properties of nanometer sized particles and need in further miniaturization of electronic devices. Today foundries that produce chips for electronic devices reached to 14 nanometer technology node. Hence, the present goal in the field of nanofabrication is to learn what happens below 10 nanometer and beyond [60].

Today there are many equipment, techniques and ways to produce nanodevices. One can select and improve the nanofabrication process according to your wishes and requirements of the scientific or technological goal. This wide spectrum of choices (like bottom-up, top-down approaches etc.) and tools (electron beam writer, focus ion beam etc.) makes the nanofabrication processes challenging and interesting.

In our work, we followed the top-down approach to construct nanopillar devices. This nanofabrication process, which was established by Dassow et al. [61] at the Jülich Research Center, consists of advanced lithography techniques like electron beam lithoghraphy (EBL), ion beam etching (IBE), photolithography, reactive ion etching (RIE), scanning electron microscopy (SEM) imaging, and deposition techniques like plasma-enhanced chemical vapor depositions (PECVD) and normal chemical vapor depositions (CVD).

However, the generation of secondary electrons during the employment of EBL and SEM makes the process of Dassow [61] inapplicable for the multilayers that are deposited on *highly* insulating substrates. For this reason the process is in this work adapted for highly insulating substrates [59].

3.1. Nanofabrication and lithography

3.1.1. Deposition of Co_2MnSi

The multilayers with Co_2MnSi (CMS) ferromagnetic layers that were investigated in this work have the following structure MgO substrate / Cr (20 nm) / Ag (60 nm) / CMS (20 nm) / Ag (8 nm) / CMS (5 nm) / Ag (2 nm) / Au (50 nm). They were prepared by employing an ultrahigh vacuum magnetron sputtering system with the base pressure below 10-^{7} Pa. The multilayer deposition was done by the group of Prof. Takanashi at the Tohoku University in Sendai, Japan [59]. First, Cr/Ag buffer layers were deposited on an MgO(001) single crystal substrate at room temperature (RT). Then, a 40 nm thick bottom CMS layer was grown at RT using a $Co_{43,7}$ $Mn_{28,0}$ $Si_{28,4}$ alloy target. The bottom CMS layer was subsequently annealed at 500^{0} C to promote chemical ordering. A 5 nm thick Ag spacer layer followed by a 5 nm thick top CMS layer were then deposited at RT. The top CMS layer was also annealed at 500^{0}C and was finally capped by Ag and Au protective layers.

3.1.2 Defining bottom electrodes and charge dissipater layer

The first part of nanofabrication process is the definition of the bottom electrodes and the formation of the dissipater layer. The role of the latter is to prevent charge accumulation during EBL and SEM by providing an electrical contact to ground potential. The raw sample stacks are cleaned first with acetone and then with propanol in an ultrasonic bath. Propanol is used to avoid acetone adheres on the capping layer. After blowing-off with gas N_2, the stacks are dehydrated on hot

plate (or oven) at 150^{0}C. After cooling to RT, the samples are ready for spin-coating (One can find different recipes and different chemicals for cleaning samples).

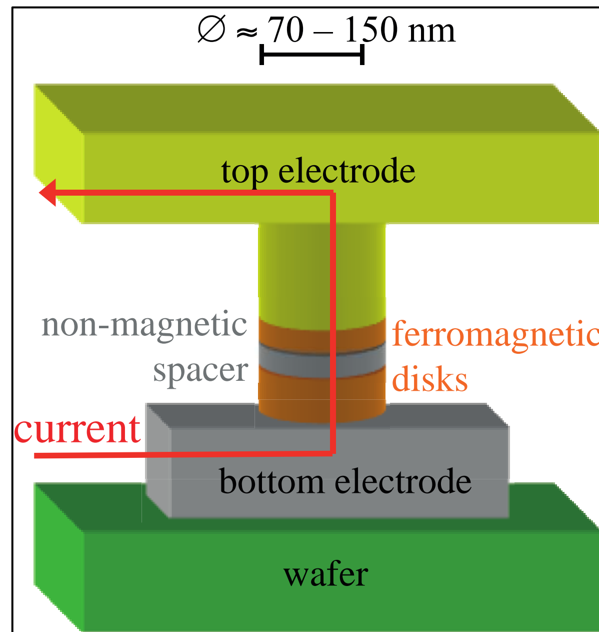

Figure 3.1: Schematic view of the nanopillar structure for current-induced magnetization dynamics experiments. The current flows between the bottom and top electrodes and thus through the two ferromagnetic layers in the nanopillar.

The stacks are mounted in the spin-coater with the proper chuck. Coating time and rotation speed have an effect on the thickness of the photoresist, which in turn affects the photoresist effect exposure dose (exposure time x intensity) in an indirect way. In our case the photoresist AZ 5214 E is used to define structures for the photolithography steps. AZ 5214E is suitable for both negative and positive (image reversal) image process. Spin-coating at 4000 rpm (cycles per minute) for 40 s results in a 1.4 µm thick AZ resist layer. According to the desired thicknesses, different coating parameters can be applied. A starting point for choosing proper parameters is the information in the manual provided by the photoresist manufacturing company, but finally the photoresist thickness was measured via profilometry tools like ellipsometry or Dektak machines.

Stacks covered with photoresist are dried on the hot plate at 90^0 C. Different recipes can be applied for drying. With the positive Cr mask shown in Figure 3.2 b the sample stacks are exposed to UV light. In this step a Süss MA-6 mask aligner is

used. Then samples are developed with AZ 400K (diluted 1:4) or AZ 326MIF developer and deionized water. It was checked with an optical microscope, whether the development is enough or not with proper light wavelength of microscope according to the property of the photoresist. It is very important to get healthy e-beam markers for the subsequent steps. As mentioned above, all these steps should be optimized with test samples. After obtaining the desired development, samples are etched with in an OXFORD Ionfab 300 Ion Beam Etcher (IBE) at an angle of incidence of 50^0 angle, 500 eV ion energy, and 44 mA beam current. The etching process is stopped before it reaches to substrate. Hence, the Cr/Ag buffer layer still covers the MgO substrate (Figure 3.2 a). Because the main goal is to leave a dissipater layer to avoid charging during EBL and SEM, it is important to use carefully calibrated etching rates to calculate the etching time. Now the samples with bottom electrodes are ready for the cleaning with acetone and propanol. A single bottom electrode is shown in Figure 3.2.c. It is also important to emphasize that all bottom electrodes are connected to each other. There are also large un-etched areas surrounding (black in Figure 3.2.b) and connecting (red in Figure 3.2.b) to the bottom electrodes, which in turns increase the surface area of the metallic dissipater. This part of the process differs from the Jülich nanopillar fabrication process [59], [60], [61]. Since in previous works GaAs substrates with larger conductivity were used, special dissipation and grounding of charge accumulation was not needed.

3.1.3 Defining nanopillars by EBL

The second level of the nanofabrication is the formation of the nanopillar structures. After cleaning and dehydration, samples are coated with hydrogen silsesquioxane (HSQ) or XR 1541, which are sensitive e-beam resists. After dehydration at 220^0 C the samples are written by a Vistec EBPG 5000 plus e-beam writer using the desired CAD file the proper dose. After tests and calibrations, the proper dose of writing was determined to be 5500 μC/cm^2. The written samples are developed with Microposit MF CD-26 developer and cleaned in the deionized water. The resulting free-standing nanopillar mask is imaged by SEM, Figure 3.3.a.

The etching is done by IBE at energy of 500 eV and a beam current of 44 mA. The angle of incidence was 10^0 and 80^0 for equal time periods to avoid redeposition and the sample was rotated. A top view SEM image of the nanopillar after etching is shown in Figure 3.3.b. Since the etching parameters of most elements are known, in general one can calculate total time etching. But in our case the etching rate of the CMS layers is not known. Therefore, the samples are etched for short time intervals and the progress is checked in between by the magneto-optical Kerr effect (MOKE). If the etching depth is not sufficient, remaining Co_2MnSi will give rise to a hysteresis loop in the MOKE measurements. Hence, etching is stopped when the hysteresis disappears indicating that the Co_2MnSi layers are completely removed.

After obtaining the desired etching depth, samples are cleaned with acetone and propanol without ultrasonic bath in order to not destroy the nanopillars. Figure 3.3.d shows the schematic cross-sections of the sample before and after IBE. The comparison of the data in Figure 3.3.a and c shows an almost perfect match between the electron beam written HSQ structure (ellipse with dimensions 75x120 nm^2) and the etched elliptical multilayer nanopillar (73x119 nm^2). This means that the dissipater layer and connections between the bottom electrodes worked properly and improved the electron beam writing process as desired.

During the IBE of the nanopillars, the remaining buffer layer parts between the individual electrodes are also etched, since they are not covered with photoresist. This reduced the area of the dissipater, which however is still efficient enough for high-resolution SEM imaging as seen in Figure 3.3.c.

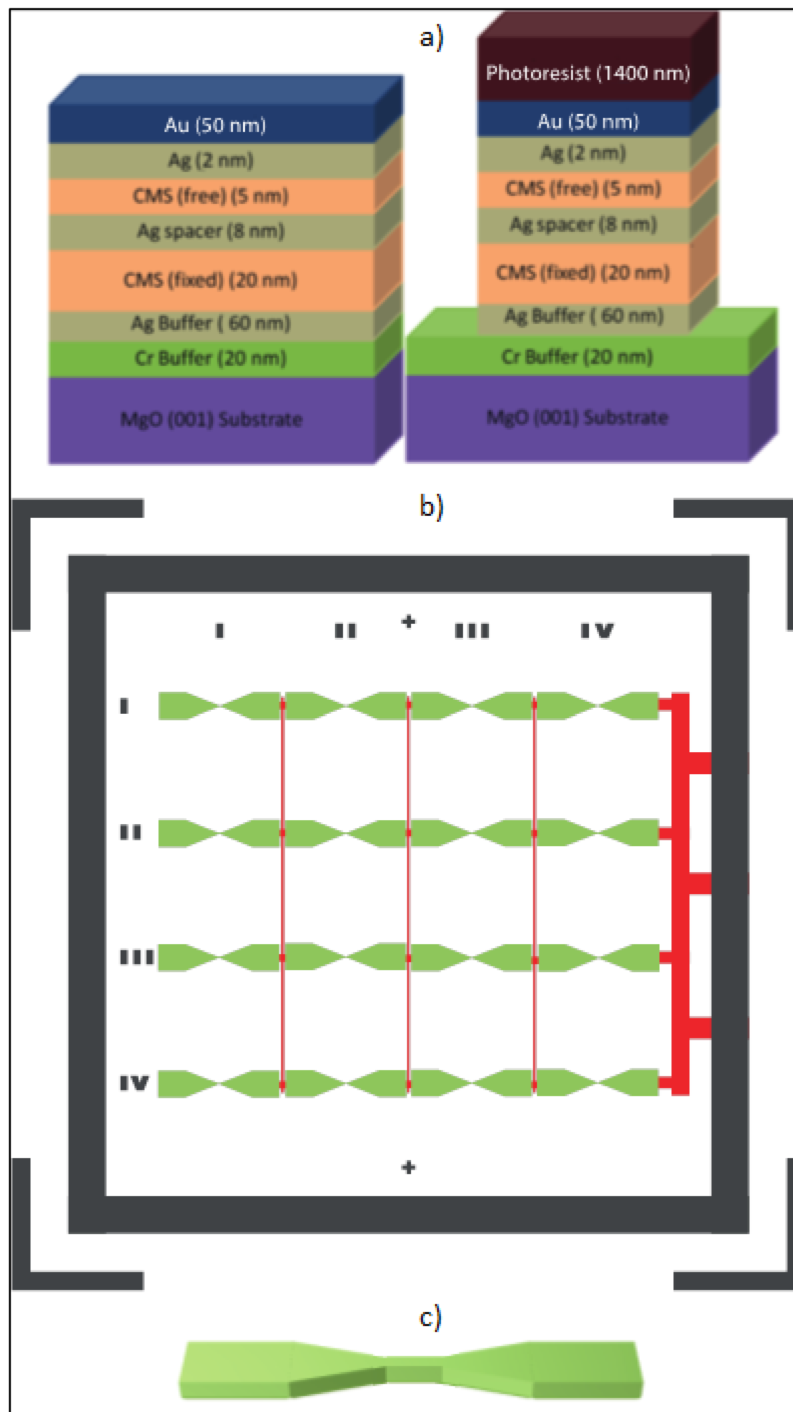

Figure 3.2: Defining nanopillars by EBL a) Cross-section view of the layer stack before (left) and after (right) partially etching the bottom electrodes. b) CAD mask (1x1 cm^2) for an array of 4x4 bottom electrodes (green) with additional elements (red) that connect all bottom electrodes to each other and to the outer frame that is connected to ground. c) Illustration of a single bottom electrode.

2.1.7. Insulation and opening contact windows

The third level of the nanofabrication is applying an insulation and opening contact windows. The main aim of this step is to protect and insulate each individual nanopillar from the environment and supply the desired area for the top electrode. This insulation layer also separates the bottom electrode from the top electrode to avoid possible short circuits. In other words, the insulation provides lateral and vertical separation. First, HSQ is coated on the samples in same way as mentioned above. This time, the whole area, where bottom electrodes are located, is exposed to the electron beam with a dose of 250 $\mu C/cm^2$ (flood exposure) to convert the HSQ film into a SiO_x-like insulating layer and to plenaries the surface [59]. Samples are developed in CD-26 and deionized water. Now there is a silicon oxide layer on the samples. As an additional insulation layer to avoid electrical short circuit, 50 nm of Si_3N_4 is deposited on the silicon oxide layer by plasma enhanced chemical vapor deposition (PECVD). After cleaning with acetone and propanol, contact windows (10x10 μm^2, Figure 3.4.a) are opened in same way as mentioned above, i.e. with AZ 5214E, Süss MA6 mask aligner, and AZ326 MIF or AZ 400K developer. Contact windows are etched with IBE at an angle of 30^0 and at reduced beam energy of 250 eV, since the energy of the ions turned out to be very critical cross-section of the sample before and after transferring the nanopillar structure to the multilayer stack. It is easier to control etching depth of the contact window at low energies. If one goes to higher energy values, there is always possibility of overetching which means destroying nanopillar structure. To control the etching process (not to etch too far) the contact windows are checked with SEM (The brand of SEM is not mentioned here, because several SEMs are used for imaging depending on availability). An example is shown in Figure 3.4.b. It is also possible to check whether the nanopillars appear in contact windows or not by Atomic Force Microscopy (AFM). But there is always the risk of breaking the nanopillars with the AFM tip, since the contact area of the nanopillars with the substrate is so small that the applied pressure from the AFM tip easily can become too high. For some materials those consist nanopillars, the etching rate is higher

than that of the materials those consist insulation layers. In this case there is a risk of developing a hole in the contact window where the nanopillars used to be (Figure 3.5). For this reason it is very important to etch at low energy and for short time periods to check the etching process.

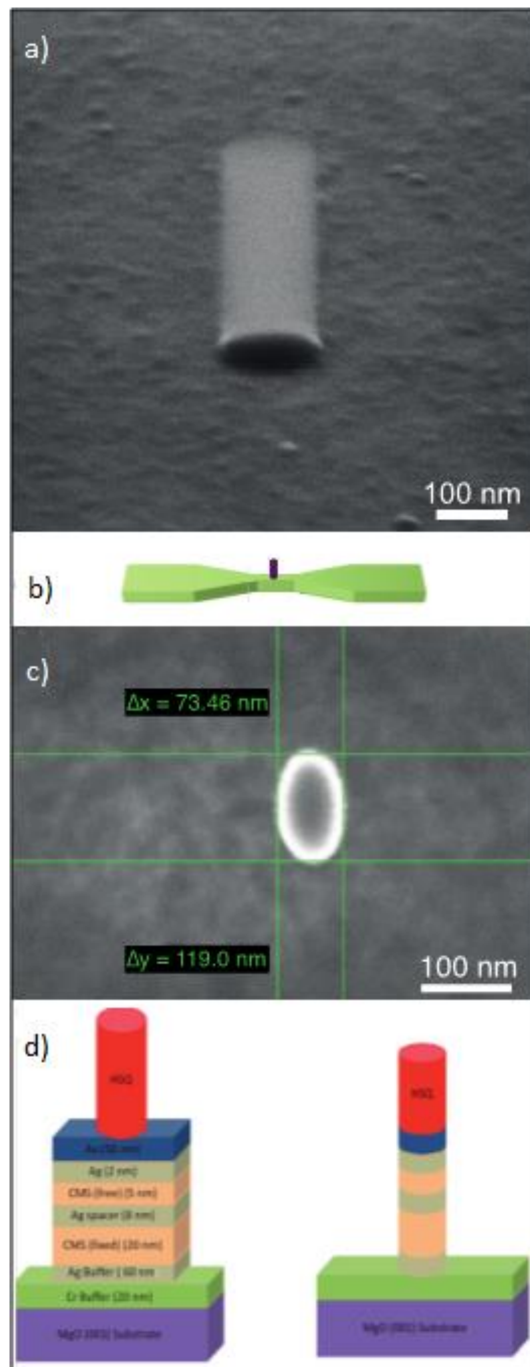

Figure 3.3: Defining nanopillar structures. a) SEM micrograph of an HSQ nanopillar defined by EBL and after development. b) Sketch of a single nanopillar on the bottom electrode. c) SEM top view SEM image of a multilayer nanopillar structure after IBE. d) Schematic of IBE process.

After getting proper results, contact windows are cleaned with reactive ion etching (RIE), to make them ready for the top electrodes deposition. It is important to remove HSQ residuals. If HSQ remains on top of the nanopillar, it will block the current between top and bottom electrodes during the measurements.

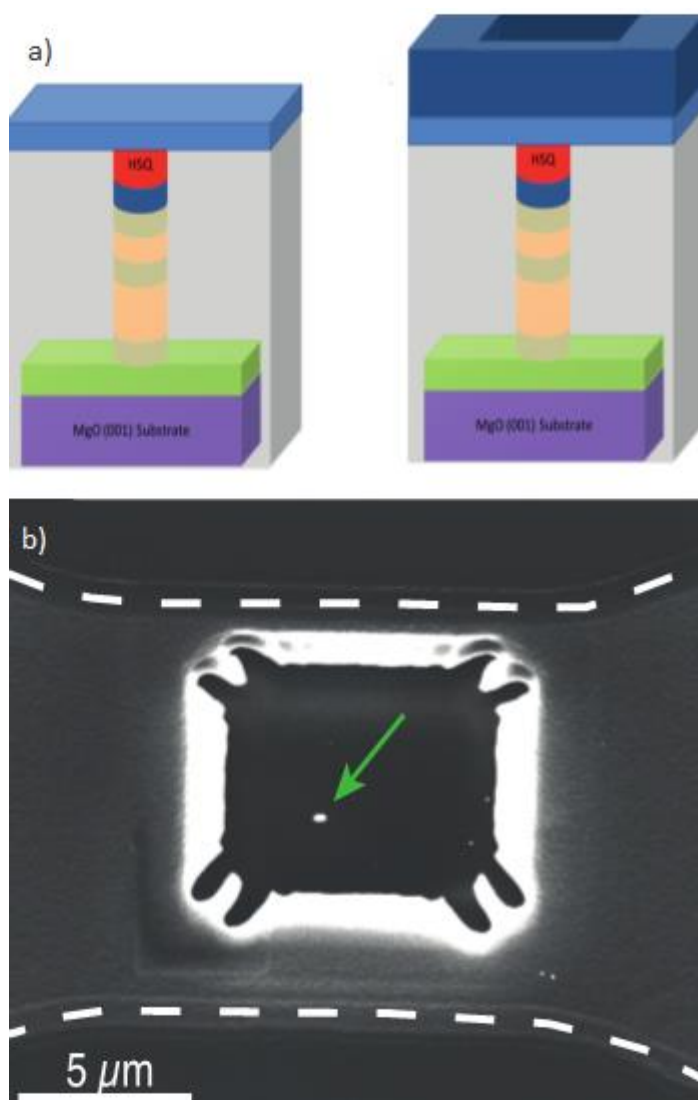

Figure 3.4: Insulation and opening contact windows a) Left: Lateral and vertical insulation of the nanopillars by electron-beam exposed HSQ (grey) and 50 nm Si_3N_4 deposited by PECVD (light blue). Right: Opening of the 10x10 μm^2 contact windows with a photoresist mask (dark blue) and IBE. b) SEM image of the 10x10 μm^2 contact window with the uncovered top of the nanopillar (green arrow).

For this reason trifluoromethane (CHF_3) plasma is used in RIE chamber. Samples are finally cleaned with acetone and propanol in an ultrasonic bath until all

photoresist residuals are removed. It turned out to be good practice to check with optical microscope whether all resist residuals are removed or not. If not, cleaning is continued until all remainders are removed. Since IBE hardens the photoresists, this takes longer than usual.

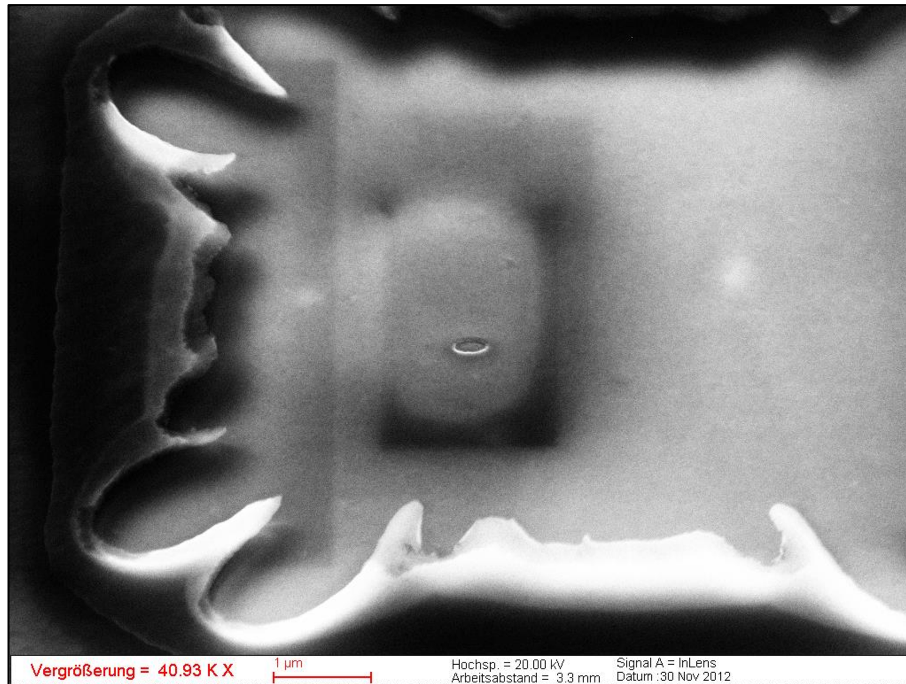

Figure 3.5: SEM view of an overetched contact window. The etching rate of capping layer of the nanopillar is higher than that of the insulators forming the contact window. For this reason the nanopillar is etched faster than the surrounding.

2.1.8. Deposition of top electrodes and removing connections

After opening the contact windows, samples are ready for the deposition of the top electrodes. Again AZ 5214E is coated and dehydrated in same manner as mentioned above, UV exposured using a Süss MA6 mask aligner, and developed with the proper developer. The Cr mask structure is shown in Figure 3.6.a.

After checking with optical microscope, if the development is sufficient, samples are ready for top electrode deposition. 15 nm Ti and 200 nm Au are deposited on the sample with a Leybold L 560 physical vapor deposition (PVD) system. Before deposition, samples are cleaned in PVD chamber to obtain desired contacts.

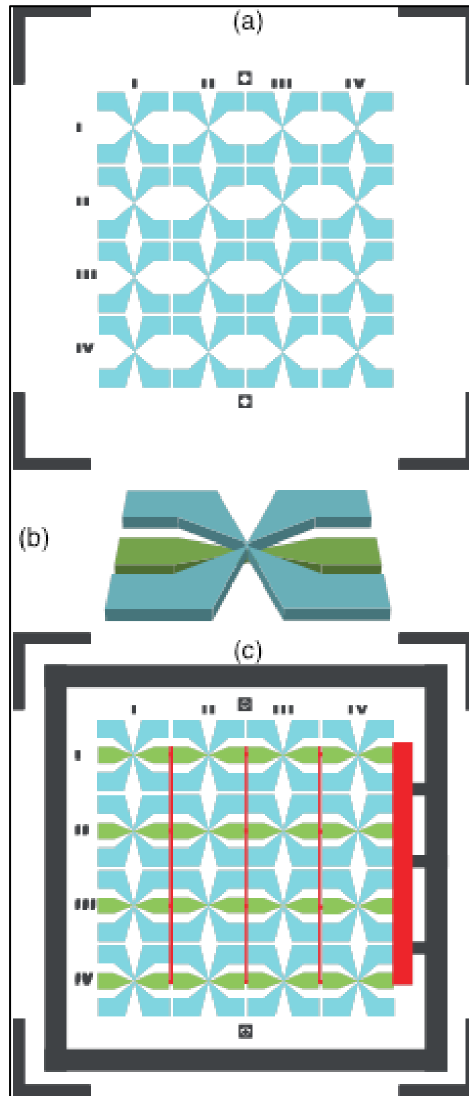

Figure 3.6: Deposition of top electrodes and removing dissipater connections. a) CAD mask for an array of 4x4 top electrodes (1x1 cm^2). b) Illustration of the top (blue) and bottom (green) electrodes of a single nanopillar device. The pillar itself is vertically sandwiched between the two electrodes. c) CAD etch mask (red elements) for the removal of connections between the devices and to the outer frame superimposed to the masks for the bottom (green) and top (blue) electrodes.

After the deposition a lift-off process is applied until all photoresist and Au layer outside of top electrodes are removed. It is recommended to check with an optical microscope to make sure that all resist is removed. Lift-off process is continued until desired bottom electrodes are obtained.

It is important to employ the lift-off process immediately. Otherwise Au particles can easily penetrate into photoresist and may stick on undesired parts of the surface, thereby possibly causing short circuits.

After deposition of top electrodes again AZ 5214E resist is coated on the samples and exposured in same manner as above using a mask consisting of the red elements in Figure 3.6.c. After sufficient development, IBE is applied to remove the connections between bottom electrodes. After a reaching MgO substrate with IBE, samples are carefully cleaned with acetone and propanol in an ultrasonic bath. If one did not etch down to the substrate in the first cycle, the etching is repeated until the substrate is reached. The sample is finally checked with an optical microscope. The single individual nanopillar devices with bottom and top electrodes are shown in Figure 3.6.b and a sketch of nanopillar structure is shown in Figure 3.1. Now the samples are ready for measurements.

3.2. Experimental setup

The measurement system for the four-probe transport measurements is designed as follows. The main part of the setup is a cryostat from Oxford Instruments placed between the poles of a Bruker B-E15f electromagnet (Figure 3.7.a). A B-EC1 Bruker power supply controls the current applied to the coils of the magnet (Figure 3.7.b)). If necessary, cooling with He_4 is possible by pumping the He inside the cryostat in the volume around the sample. An ITC 503 temperature controller is used to stabilize the temperature. In this study, all the measurements were done at RT.

A Keithley 6430 sourcemeter is used to apply the DC current to sample and at the same time serves as multimeter that measures the resistance of the sample. A Magnet-Physik FH-55 Hall probe measures the magnetic field between the poles of the electromagnet. All this equipment is connected to a desktop computer and a

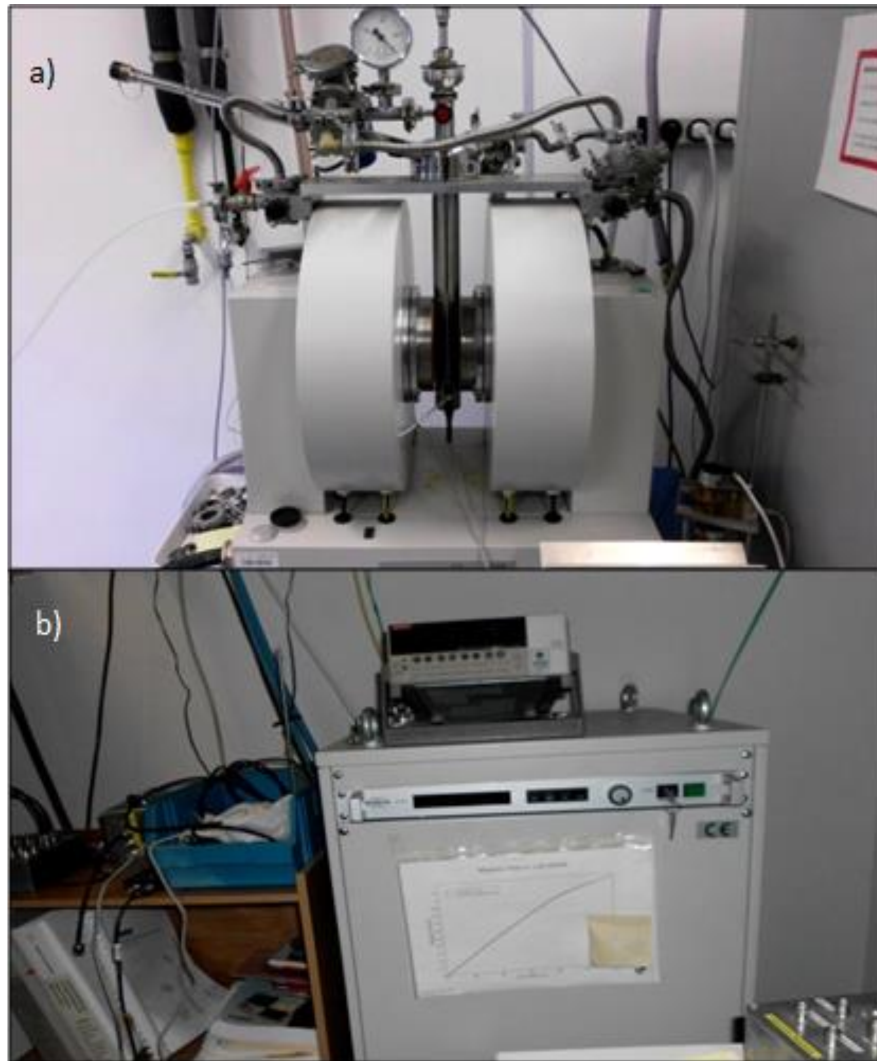

Figure 3.7: Measurements system with a) the electromagnet with the cryostat between its poles and b) the power supply of the electromagnet.

special programme written with Labview runs the measurements. The sample is glued to specially designed sample holder, which has ten pins that can be easily plugged into a home-built cryostat insert. Since the sample holder has ten pins, the insert has also ten wires that fit to the sample holder. The insert can be adjusted in the cryostat according to the desired orientation with respect to the magnetic field. To get right orientation, it is important to glue in right position in order to get right field orientation for the measurements (The magnetic field is applied in the direction parallel to pins of the sample holder).

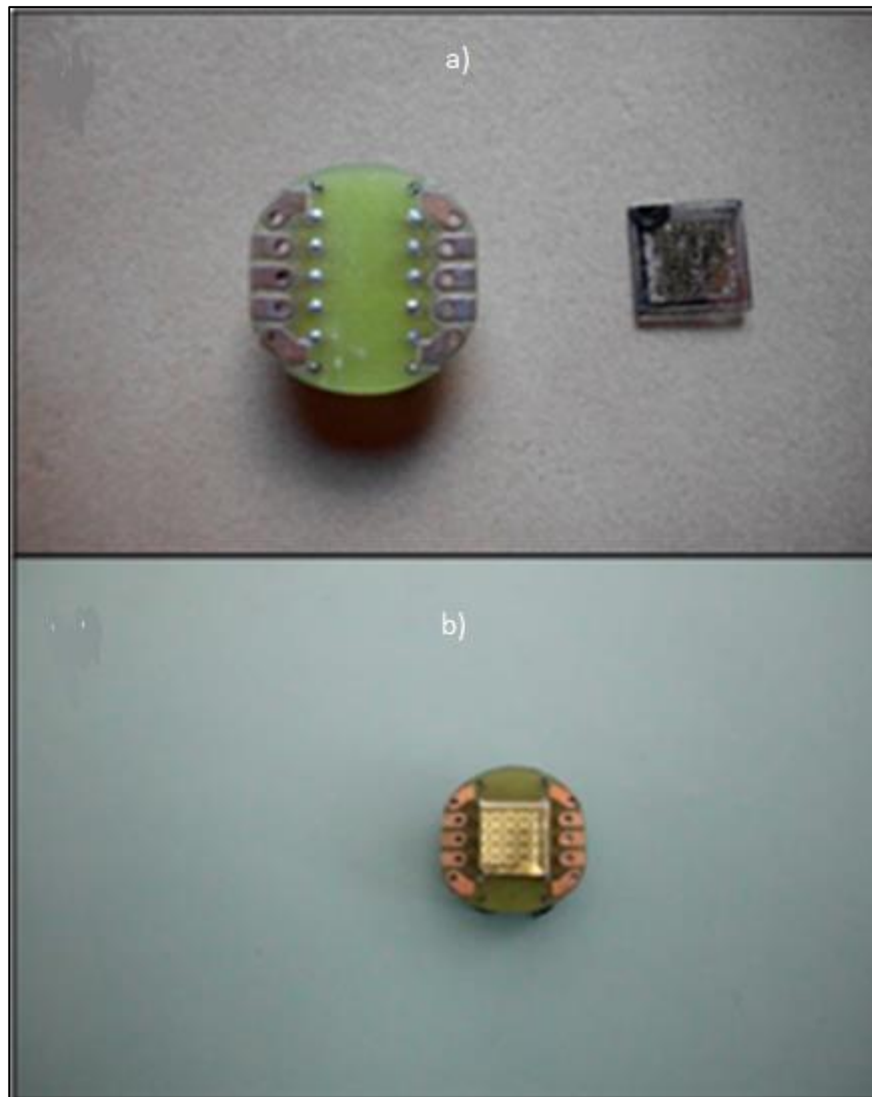

Figure 3.8: Preparation of the sample for measurements: Sample and sample holder (chip carrier) before a) and after b) gluing the sample onto the sample holder.

The electrodes of the sample are bonded to pads of the sample holder with edge type wire bonder. The cables coming from cryostat insert lead at the outside to a box, where one can select the pads to be used during measurements. Detailed information can be found in previous works [63],[64].

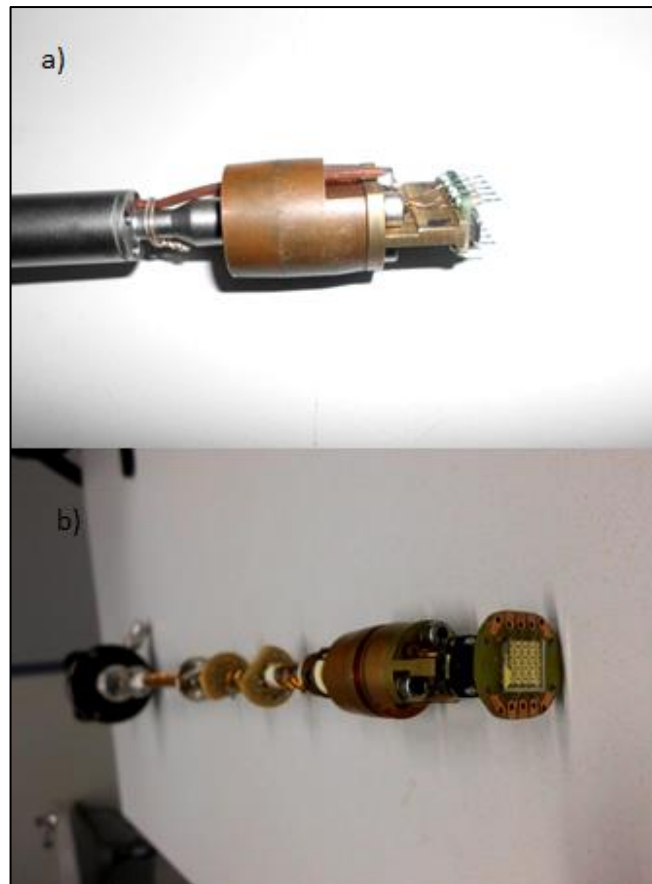

Figure 3.9: Sample holder with special chip carrier. a) Front end of the cryostat insert with the ten-pins connector. b) Complete cryostat insert with a sample holder plugged into the connector. The bonding wires between the electrodes of the sample and the pads of sample holder can hardly be seen.

3.3. GMR and Current Induced Magnetization Switching

In this section, we present the results that are obtained from measurements after successful modification of nanopillar lithography process. These results are divided into two groups. First group will be about GMR measurements of nanopillars with different diameters. There will be also results of measurements those are obtained from different directions of applied magnetic field. Second group of results will be about current induced magnetization switching of nanopillar structures. In this chapter, every given measurements are obtained at room temperature.

3.3.1. GMR Results

The resistance is measured in a four probe configuration. Current goes from bottom electrode to top electrode. After the successful application of modified nanofabrication process for high insulating substrates, in Figure 3.10 we present measurements of magnetoresistance versus DC magnetic field. Magnetic field is applied in the plane of the sample either parallel to the long (Figure 3.10.a) or short (Figure 3.10.b) axis of the elliptical cross section of the nanopillar structure. As mentioned above, the resistance is measured in a 4-probe configuration. A DC current $I_{DC} = 0.1$ mA is applied between contact pads I^+ and I^- of the top and bottom electrode which is bonded by wire bonder to sample holder. The voltage drop ΔV is measured at the contact pads V^+ and V^- (inset of Figure 3.10 a). The resistance is then given by $R = \Delta V/I_{DC}$. During sweeping the magnetic field for both field directions a resistance change of about $(R_{max}-R_{min})/R_{min} \approx 2\%$ due to the GMR effect is observed.

Close to zero applied field, because of the dipolar (stray field) interaction between the two ferromagnetic layers, an antiparallel alignment of the layers' magnetizations is observed. This antiparallel alignment gives rise to an increase in resistance as compared to the parallel configuration reached at large positive or negative fields. In other words, different curves that are obtained from different direction of applied field are originated from magnetic anisotropy of the sample.

From Figure 3.10.a, it is seen that the magnetic easy axis of the anisotropy is parallel to the long axis of the ellipse. A field of about ±18 mT in the opposite direction of the magnetization is needed to overcome the anisotropy barrier for magnetization reversal. In Figure 3.10.b the field is applied along the hard axis and we observe a sharp step-like change at about ±2 mT followed by a monotone variation with increasing field strength up to about 40 mT.

The initial drop of resistance is most likely related to cubic magnetocrystalline anisotropy of the singe-crystalline $Co_2MnSi(001)$ layers with easy axes at approximately ±45° with respect to the principal axes of the ellipse yielding at about ±2 mT an angle of 90° between the magnetizations of the two Co_2MnSi layers and,

thus, a resistance value half way between resistance maximum and minimum. The smooth variation of the resistance between ±(2 and 40) mT reflects the gradual rotation of the magnetizations into the direction of the applied field, which is the hard axis of the shape anisotropy

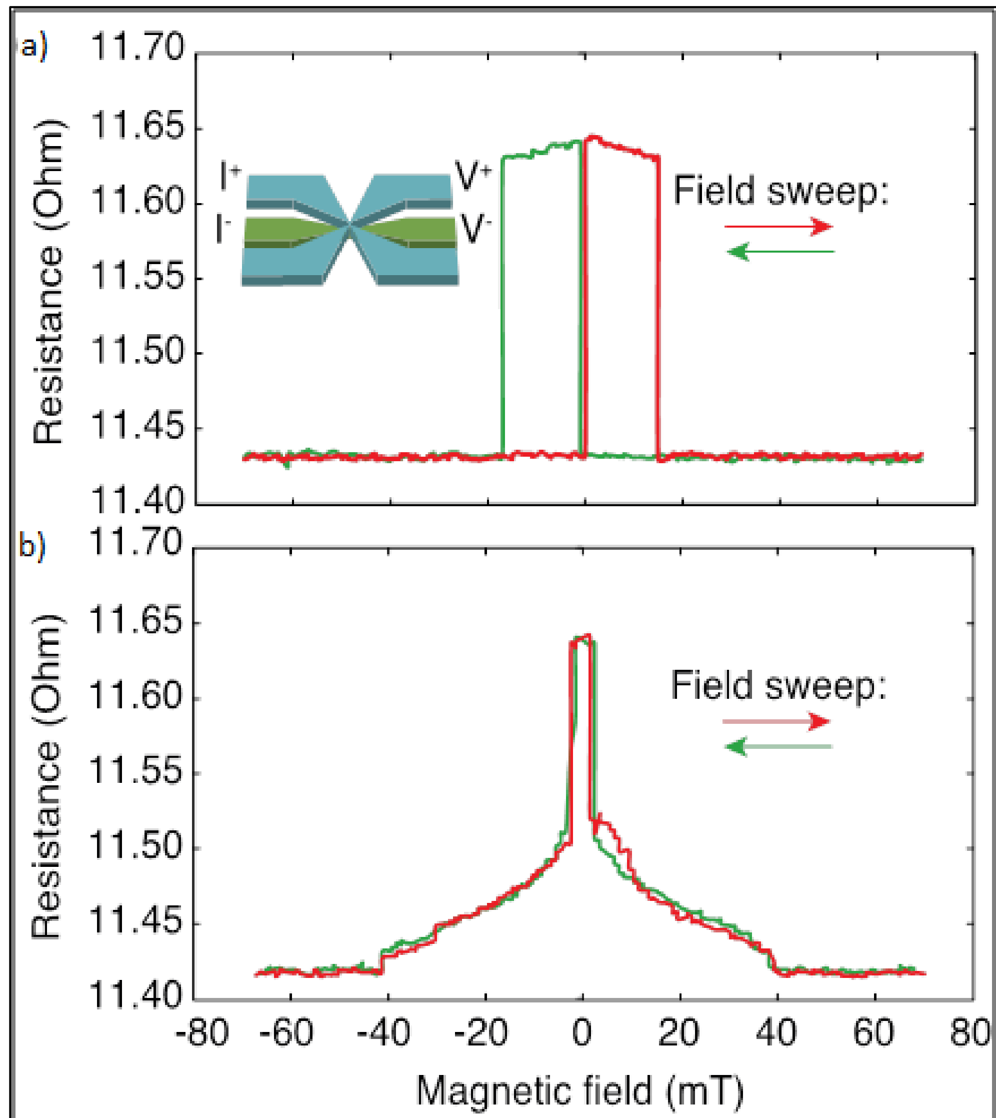

Figure 3.10: Giant magnetoresistance measurement at room temperature of nanopillar with cross section of 75x120 nm^2 .Applied current is 0.1 mA. The magnetic field is applied in the sample plane and parallel to the (a) long axis direction and b) short axis direction of the elliptical cross-section. Red and green curves indicate increase and decrease in the field sweep. The inset in a) shows the electrical contacting for the 4-probe measurements.

3.3.2. Current-induced magnetization switching results

The resistance is measured in a four probe configuration as in GMR measurements. Current goes from bottom electrode to top electrode and vise versa. Figure 3.11 presents current induced magnetization reversal measurements (resistance versus current). Magnetic field is not applied neither parallel to the long nor short axis of the elliptical cross section of the nanopillar structure. As mentioned above, the resistance is measured in a 4-probe configuration. A DC current $I_{DC} = \pm 3$ mA is applied between contact pads I^+ and I^- of the top and bottom electrode which is bonded by wire bonder to sample holder. Sweeping of current starts from -3 mA and reaches to 3 mA then returns to -0.3 mA. The voltage drop ΔV is measured at the contact pads V^+ and V^-. The resistance is then given by $R = \Delta V / I_{DC}$

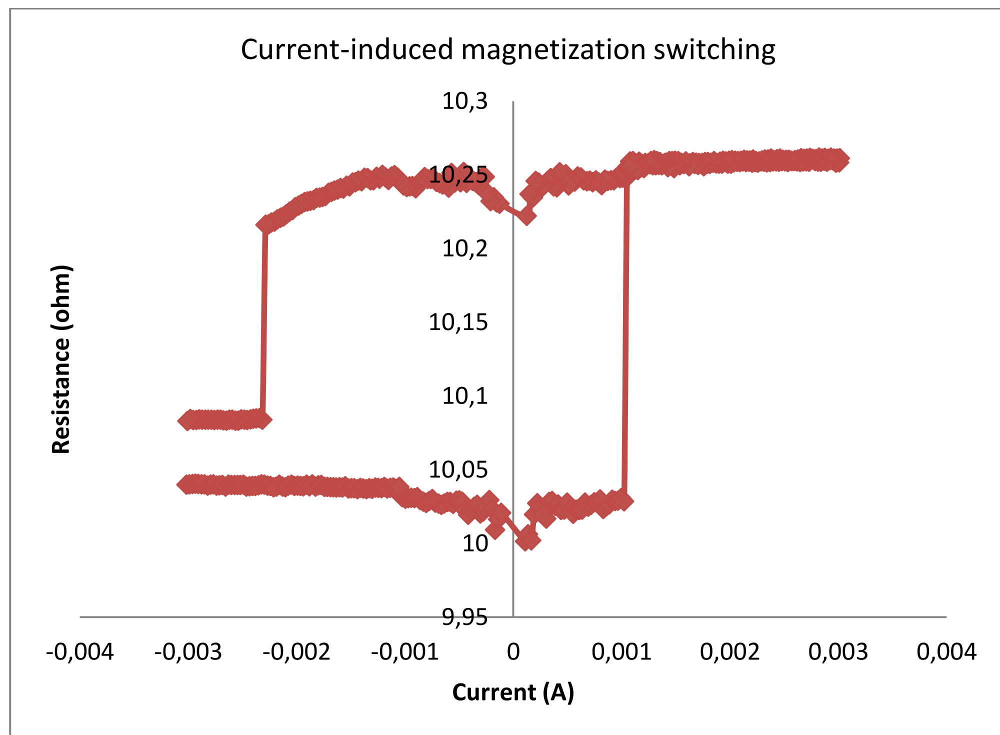

Figure 3.11: Current–induced magnetization switching experiment at room temperature of nanopillar with cross section of 75x120 nm^2 without applied magnetic field. Current sweep starts from -0.003 A and reaches to 0.003 A. Hysteris behavior of resistance is observed at current values between -0.0025 and 0.001 A.

At -0.22 mA, because of spin transfer torque effect, magnetization of ferromagnetic layers becomes antiparallel. Sudden increase in the resistance of the system is observed. On the opposite direction of the current sweep, at 1.1 mA, because of spin transfer torque effect, magnetization of ferromagnetic layers become parallel. The resistance of the system drops. Because of Joule heating in the system, gap between the resistance of the system (at the beginning and end values) is observed.

4. DISCUSSION AND CONCLUSION

In this thesis, we have focused on nanofabrication of spintronic devices and developed a new process technique to solve the charging problem. Then we have investigated GMR properties and the current induced magnetization reversal by spin transfer torque in single nanopillar of $Co_2MnSi/Ag/Co_2MnSi$ multilayer structure. Main reasons for choosing Co_2MnSi are, high Curie (above room temperature) temperature and high spin polarization. These two parameters are crucial for spintronic device applications.

In the beginning of this work, we had encountered high charging problem due to insulating MgO substrate during the electron beam writing and imaging individual nanopillar structures. In the previous works the researchers have not encountered these problems since the samples were deposited on semiconductor or conductor substrates in Jülich Research Center. In contrast, in this work we have to use insulating substrates and we have encountered highly charging problem. In order to solve this problem in this study '*Jülich nanopillar fabrication process*' has been modified for insulating substrates. As a solution, we have developed new technique for charging substrates and we have designed new Cr photomasks for photolithography which has bottom electrodes connected to each others to increase conducting area on the sample surface. In addition to change in the mask design, we have kept Cr and Ag layer on the substrate not etched with ion beam etcher at the definition of bottom electrodes, they continued to serve dissipation layer during electron beam writing of nanopillars. Before measurements, as an additional step, all the connections between nanopillars and dissipation layer were etched away to avoid short circuit.

The sample was bonded to sample holder with wedge type wire bonder, before imaging with scanning electron microscope. With these modifications, charging obstacle due to insulating substrates was overcome, and successful nanopillars were nanofabricated. In the third chapter, detailed information about new nanofabrication process is given in step by step. We have presented experimental results obtained from transport measurements of the nanopillars that

were nanofabricated with '*new Jülich nanofabrication process'*. Experimental results were divided into two groups. In the first part, GMR measurements of applied magnetic field with different angles are shown. In second part, current induced magnetization reversal measurements of different nanopillars are presented.

If we summarize the work done in this thesis briefly : We have encountered highly charging problem due to MgO substrate during e-beam writing and imaging nanopillars. To overcome this charging effect, we have designed new mask to reduce charge accumulation. Additionally, we have kept all the bottom electrodes unetched to increase conducting area. After depositing top electrodes, we have etched all connections and unetched parts. After successful modification of Jülich nanopillar fabrication process we have studied GMR measurements and current induced magnetization reversal measurements.

There are several works that have been done up to this study and during this study. Sakuraba and his colleagues from Tohoku University, Japan, have investigated similar multilayer structure of $Co_2MnSi/Ag/Co_2MnSi$. In their work they employed extended layer nanopillar structure [65]. In addition they have studied computer simulations. Details can be found [66]. On the other hand, there are also similar studies on multilayer structure of Co_2MnSi Heusler alloy with different nonmagnetic layers like Cr [67].

Dividing future works into three groups is possible. First group of future work, as it was mentioned in the second chapter, high frequency oscillations induced by spin transfer torque is very important field of research. STO measurements could be done with the samples that are prepared with modified nanofabrication process. High frequency measurements and comparison of the samples with different radii could be separate topic for future studies. It would be interesting to extend studies on vortex dynamics in Co_2MnSi layers.

Second group of possible works can be related to studies of modified structure of the multilayer. It will be interesting to investigate different thickness of Ag layers between Co_2MnSi layers. It is also possible to change the thicknesses of Co_2MnSi layers. As it was mentioned in theory chapter, tunnel junctions give higher magnetoresistance values. For future work one can change Ag layer with suitable thin insulator layer like MgO or AlO_x.

Third group of future works is micromagnetic simulation of nanopillars in the present work and comparison of our experimental results with simulation results. Nowadays, micromagnetic simulations gained acceleration and attracted many scientists to itself. Many programme packages for simulations for magnetism were coded and still there are lots of extensions for these codes are being written.

Here we mentioned possible directions of a number of future works for Co_2MnSi nanopillar geometries those were fabricated with modified Jülich nanofabrication process. There are a number of different Hesuler alloys with outstanding properties for spintronic applications. It would be interesting for instance to study tetragonal Heusler alloys, like Mn_3Ga, which are good candidates for spin transfer torque based applications due to high spin polarization and high Curie temperature [68].

REFERENCES

[1] Baibich M. N., Broto J. M., Fert A., Nguyen Van Dau F., Petroff F., Eitenne P., Creuzet G., Friederich A., Chazelas J., (1988), "Giant Magnetoresistance of (001)Fe/(001)Cr Magnetic Superlattices." Physical Review Letters, 61, 2472-2475.

[2] Binasch G., Grünberg P, Saurenbach F., Zinn W., (1989), "Enhanced magnetoresistance in layered magnetic structures with antiferromagnetic interlayer exchange." Physical Review B, 39, 4828-4830.

[3] Parkin S. S. P., More N., Roche K. P., (1990), "Oscillations in exchange coupling and magnetoresistance in metallic superlattice structures: Co/Ru, Co/Cr, and Fe/Cr" Physical Review Letters, 64, 2304-2308.

[4] Slonczewski J.C., (1996), Current-driven excitation of magnetic multilayers." Journal of Magnetism and Magnetic Materials, 159, L1-L6.

[5] Berger L., (1996), "Emission of spin waves by a magnetic multilayer traversed by an electric current." Physical Review B, 54, 9353.

[6] Tsoi M., Jansen A. G. M., Bass J., (1998), "Excitation of a magnetic multilayer by an electric current" Physical Review Letters, 80, 4281–4284.

[7] Sun J.Z, (1999), " Current-driven magnetic switching in manganite trilayer junctions ", Journal of Magnetism and Magnetic Materials, 202, 157–162.

[8] Myers E. B., Ralph D. C., Katine J. A., Louie R. N., Buhrman R. A., (1999), "Current-Induced Switching of Domains in Magnetic Multilayer Devices." Science, 285, 867-870.

[9] Kiselev S. I., Sankey J. C., Krivorotov I. N., Nemley N. Schoelkopf C., R. J., Buhrman R. A., Ralph D. C., (2003), "Microwave oscillations of a nanomagnet driven by a spin-polarized current.", Nature, 425, 380-383.

[10] Katine J. A., Albert F. J., Buhrman R. A., Myers E. B., Ralph D. C., (2000), "Current-Driven Magnetization Reversal and Spin-Wave excitations in Co/Cu/Co Pillars." Physical Review Letters, 84, 3149-3152.

[11] Dassow H., Lehndorff R., Bürgler D.E., Buchmeier M., Grünberg P.A., Schneider C.M., van der Hart A., (2006), "Normal and inverse current-induced magnetization switching in a single nanopillar" Applied Physics Letters, 89, 222511.1-3.

[12] Thomson W., (1856), "On the electro-dynamic qualities of metals: Effects of magnetization on the electric conductivity of nickel and of iron" Proceedings of Royal Society of London, 8:546-550.

[13] N. F. Mott, (1936), "The resistance and thermoelectric properties of the transition metals," Proceedings of the Royal Society of London. Series A, Mathematical and Physical Sciences, 156, 368-382.

[14] Valet T., Fert A., (1993),"Theory of the perpendicular magnetoresistance in magnetic multilayers." Physical Review B, 48, 7099-7113.

[15] Julliere M., (1975), "Tunneling between ferromagnetic films," Physics Letters A, 54A, 225-226.

[16] Miyazaki T., Tezuka N., (1995), "Giant magnetic tunneling effect in Fe/Al_2O_3/Fe junctions", Journal of Magnetism and Magnetic Materials, 139, L231-L234.

[17] Moodera J. S., Kinder L. R., Wong T. M., Meservey R., (1995), "Large magnetoresistance at room temperature in ferromagnetic thin film tunnel junctions", Physical Review Letters, 74, 3273-3276.

[18] Yuasa S., Nagahama T., Fukushima A., Suzuki Y., Ando K., (2004), "Giant room temperature magnetoresistance in single-crystal Fe/MgO/Fe magnetic tunnel junctions", Nature Materials, 3, 868-871.

[19] Parkin S. S. P., Kaiser C., Panchula A., Rice P. M., Hughes B., Samant M., Yang S.-H., (2004), "Giant tunnelling magnetoresistance at room temperature with MgO (100) tunnel barriers", Nature Materials, 3, 862-867.

[20] Berger L., (1984), "Exchange Interaction between Ferromagnetic Domain Wall and Electric Current in Very Thin Metallic Films" Journal of Applied Physics, 55, 1954-1956.

[21] Freitas P. P., Berger L., (1985), "Observation of s-d exchange force between domain walls and electric current in very thin Permalloy films" Journal of Applied Physics, 57, 1266-1269.

[22] Hung C.-Y., Berger L., (1988), "Exchange forces between domain wall and electric current in permalloy films of variable thickness" Journal of Applied Physics, 63, 4276-4278.

[23] Slonczewski J. C., (1989), "Conductance and exchange coupling of two ferromagnets separated by a tunneling barrier", Physical Review B , 39, 6995-7002.

[24] Wegrowe J.E., Kelly D., Jaccard Y., Guittienne P., Ansermet J., (1999), "Current-induced magnetization reversal in magnetic nanowires", Europhyics Letters, 45, 626-630.

[25] Fuchs G.D., Emley N.C., Krivorotov I.N., Braganca P.M., Ryan E.M., Kiselev S.I., Sankey J.C., Katine J.A., Ralph D.C., & Buhrman R.A.," Spin-transfer effects in nanoscale magnetic tunnel junctions." (2004), Applied Physics Letters, 85, 1205-1207.

[26] Huai Y., Albert F., Nguyen P., Pakala M., & Valet T., (2004), "Observation of spin transfer switching in deep submicron-sized and low-resistance magnetic tunnel junctions", Applied Physics Letters, 84, 3118-3120.

[27] Grollier J., Lacour D., Cros V., Hamzic A., Vaures A., Adam D., Faini G., Fert A., (2002), "Switching the magnetic configuration of a spin valve by current induced domain wall motion", Journal of Applied Physics, 92, 4825-4829.

[28] Klaui M., Vaz C.A.F., Wernsdorfer W., Faini G., Cambril E., Heyderman L.J., & Bland J.A.C., (2003), "Domain wall motion induced by spin polarized currents in ferromagnetic ring structures ", Applied Physics Letters, 83, 105-108.

[29] Tsoi M., Fontana R.E., Parkin S.S.P., (2003), "Magnetic domain wall motion triggered by an electric current", Applied Physics Letters, 83, 2617-2620.

[30] Stiles M.D., A. Zangwill, (2002), "Anatomy of spin-transfer torque", Physical Review B , 66, 014407.

[31] Ralph D., Stiles M., (2008), "Spin transfer torques", Journal of Magnetism and Magnetic Materials, 320, 1190-1216.

[32] Hillebrands B., Thiaville A., (2006), "Spin Dynamics in Confined Magnetic Structures III, Topics Appl. Physics" 101, Springer-Verlag Berlin Heidelberg.

[33] Katine J., Fullerton E.E., (2008), "Device implications of spin-transfer torques", Journal of Magnetism and Magnetic Materials, 320, 1217-1226.

[34] (web1,2015) www.everspin.com/mram (04.02.2015)

[35] Heusler F, Starck W, Haupt E., (1903), Verh DPG, 5, 220.

[36] Potter H. H., (1934), "The Magneto-Caloric Effect and Other Magnetic Phenomena in Iron" , Proceedings of the Royal Society of London, 146, 362-387.

[37] Bradley A. J., Rodgers J. W., (1934), "The Crystal Structure of the Heusler Alloys", Proceedings of the Royal Society of London, 144, 340-359.

[38] Felser C., Fecher G. H., Balke B., (. 2007), "Spintronics: a Challenge for Material Science and Solid State Chemistry", Angewante Chemie, 119, 680-699.

[39] Kainuma R., Imano Y., Ito W., Sutou Y., Morito H., Okamoto S., Kitakami O., Oikawa K., Fujita A., Kanomata T., Ishida K., (2006), " Magnetic-field-induced shape recovery by reverse phase transformation", Nature , 439, 957-960.

[40] Chadov S., Qi X., Kübler J., Fecher G. H., Felser C., S. Zhang C., (2010), "Tunable multifunctional topological insulators in ternary Heusler compounds", Nature Materials , 9 , 541-545.

[41] Lin H., Wray L. A., Xia Y., Xu S., Jia S., Cava R. J., Bansil A., Hasan M. Z., (2010), "Half-Heusler ternary compounds as new multifunctional experimental platforms for topological quantum phenomena", Nature Materials , 9, 546-549 .

[42] Franz M., (2010), "Topological insulators: Starting a new family", Nature Materials , 9, 536-537.

[43] Krenke T., Duman E., Acet M., Wassermann E. F., Moya X., Mañosa L., Planes A., (2005), "Inverse magnetocaloric effect in Ni-Mn-Sn alloys" Nature Materials. , 4, 450-454.

[44] Takeuchi I., Famodu O. O., Read J. C., Aronova M. A., Chang K.-S., C, Craciunescu, Lofl S. E., Wuttig M., Wellstood F. C., Knauss L., Orozco A., (2003), "Identification of novel compositions of ferromagnetic shape-memory alloys using composition spreads", Nature Materials , 2, 180-184.

[45] Tirpanci S., Galanakis I., Sasioglu E., (2013), "Design of half-metallic Heusler-based superlattices with vanishing net magnetization." Journal Applied Physics, 113, 043912, 1-4.

[46] de Groot R., Mueller F., van Engen P., Buschow K., (1983), "New Class of Materials: Half-Metallic Ferromagnets" Physical Review Letters, 50, 2024-2027,

[47] Park, J.H., Vescovo, E., Kim, H.J., (1998), " Direct evidence for a half-metallic ferromagnet." Nature, 392, 794-796.

[48] Ishida S., Fujii S., Kashiwagi S., Asano S., (1995), "Search for Half-Metallic Compounds in Co2MnZ (Z=IIIb,IVb,Vb Element)", Journal of Physical Saciety of Japan, 64, 2152-2157.

[49] Webster P., (1971), "Magnetic and chemical order in Heusler alloys containing cobalt and manganese ", Journal of Physical Chemistry of Solids, 32, 1221-1231.

[50] S. Kammerer, (2004), "The Heusler alloy Co2MnSi in thin films", Doctorate. thesis, Universitat Bielefeld.

[51] Brown P.J., K.V., Websteand P.J., Zieback K.R.A., (2000), "The magnetization distributions in some Heusler alloys proposed as half-metallic ferromagnets" Journal of Physics: Condensed Mater, 12, 1827-1835.

[52] Cheng S.F., Nadgorny B., Bussman K., Carpenter E.E., Das B.N., Trotter G., Raphael M.P.,Harris V.G., (2001), "Growth and magnetic properties of single crystal Co2MnX (X=Si,Ge) Heusler alloys "IEEE Transactions on Magnetics, 37, 2176-2178.

[53] Ritchie L., Xiao G., Y. Ji, Chen T.Y., Chen C.L., Zhang M., Chen J., Liu Z., Wu G., Zhang X.X., (2003) , "Magnetic, structural, and transport properties of the Heusler alloys Co_2 MnSi and NiMnSb" Physical Review B, 68, 104430, 1-6.

[54] Singh L.J., Barber Z.H., Miyoshi Y., Branford W.R., Cohen L.F., (2004)," Investigation of the growth an d magn etic properties of highly oriented films of the Heusler alloy Co_2MnSi on GaAs(001)" J.ournal of Applied Physics, 95, 7231-7235.

[55] Geiersbach U., Bergmann A., Westerholt K., (2002), "Preparation and structural properties of thin films and multilayers of the Heusler compounds Cu_2MnAl, Co_2MnSn, Co_2MnSi and Co_2MnGe " , Journal of Magnetism and Magnetic Materials , 425, 226-232.

[56] Moodera J., Mathon G., (1999), "Spin polarized tunneling in ferromagnetic junctions", , Journal of Magnetism and Magnetic Materials, 200, 248-273.

[57] Galanakis I., Dederichs P., Papanikolaou N., (2002), "Slater-Pauling behavior and origin of the half-metallicity of the full-Heusler alloys", Physical Review B, 66, 174429 1-5.

[58] Tırpancı Ş., Bürgler D. E., Schneider C. M., Rameev B., Aktaş B., (2015) "Charging effect reduction in electron beam lithography and observation of single nanopillars on highly insulating substrates." Microelectronics Engineering, 140, 33-37.

[59] (web2,2015) www.mtl.mit.edu/mems/documents/KB-forwasserman (04.05.2015)

[60] Dassow H., Lehndorff R., Bürgler D.E., Buchmeier M., Grünberg P.A., Schneider C.M., van der Hart A., (2006), "Normal and inverse current-induced magnetization switching in a single nanopillar " Applied Physics Letters, 89, 222511 1-3.

[61] Okura R., Sakuraba Y., Seki T., Izumi K., Mizuguchi M., Takanashi K., (2011), "High-power rf oscillation induced in half-metallic Co_2MnSi layer by spin-transfer torque ", Applied Physics Letters, 99, 052510 1-3.

[62] Lehndorff R., (2008), “Strominduzierte Magnetisierungsdynamik in einkristallinen Nanosaulen.” Doctorate Dissertation, Universitat zu Köln.

[63] Sluka V., (2011) “Spin-Transfer Torque Induced Dynamics of Magnetic Vortices in Nanopillars”, Doctorate Dissertation, Universitat zu Köln.

BIOGRAPHY

Şaban TIRPANCI was born in Germencik, AYDIN in 1979. He finished primary and secondary school in Aydın then went to Izmir for high school. After finishing high school, he entered Ege University Physics department for bachelor's degree. For master study he attend Fatih University Physics department. In that time period he worked as teaching assistant in Bahçeşehir University.

In 2009, he started his PhD at Graduate School of Natural and Applied Sciences, Gebze Institute of Technology under the supervision of Prof Dr Bekir AKTAŞ. He is still investigating magnetic nanomaterials with his supervisor.